HHS Public Access

Author manuscript

Nat Cell Biol. Author manuscript; available in PMC 2016 November 23.

Published in final edited form as:

Nat Cell Biol. 2016 June ; 18(6): 645–656. doi:10.1038/ncb3357.

The metabolic co-regulator PGC1α suppresses prostate cancer metastasis

Veronica Torrano[#1], **Lorea Valcarcel-Jimenez**[#1], **Ana Rosa Cortazar**[1], **Xiaojing Liu**[2], **Jelena Urosevic**[3], **Mireia Castillo-Martin**[4,5], **Sonia Fernández-Ruiz**[1], **Giampaolo Morciano**[6], **Alfredo Caro-Maldonado**[1], **Marc Guiu**[3], **Patricia Zúñiga-García**[1], **Mariona Graupera**[7], **Anna Bellmunt**[3], **Pahini Pandya**[8], **Mar Lorente**[9], **Natalia Martín-Martín**[1], **James David Sutherland**[1], **Pilar Sanchez-Mosquera**[1], **Laura Bozal-Basterra**[1], **Amaia Zabala-Letona**[1], **Amaia Arruabarrena-Aristorena**[1], **Antonio Berenguer**[10], **Nieves Embade**[1], **Aitziber Ugalde-Olano**[11], **Isabel Lacasa-Viscasillas**[12], **Ana Loizaga-Iriarte**[12], **Miguel Unda-Urzaiz**[12], **Nikolaus Schultz**[13], **Ana Maria Aransay**[1,14], **Victoria Sanz-Moreno**[8], **Rosa Barrio**[1], **Guillermo Velasco**[9], **Paolo Pinton**[6], **Carlos Cordon-Cardo**[4], **Jason W. Locasale**[#2], **Roger R. Gomis**[#3,15], and **Arkaitz Carracedo**[1,16,17,18]

[1]CIC bioGUNE, Bizkaia Technology Park, 801[a] bld., 48160 Derio, Bizkaia, Spain

[2]Department of Pharmacology and Cancer Biology, Duke Cancer Institute, Duke Molecular Physiology Institute, Duke University School of Medicine, Durham, North Carolina 27710, USA

[3]Oncology Programme, Institute for Research in Biomedicine (IRB-Barcelona), The Barcelona Institute of Science and Technology, Barcelona 08028, Catalonia, Spain

[4]Department of Pathology, Icahn School of Medicine at Mount Sinai, New York, New York, USA

[5]Department of Pathology, Fundação Champalimaud, Lisboa, Portugal.

[18]Correspondence to: Arkaitz Carracedo, acarracedo@cicbiogune.es.

The authors declare no conflict of interest.

Authors' contributions

VT and LV-J performed the majority of *in vitro* and *in vivo* experiments, unless specified otherwise. ARC carried out the bioinformatic and biostatistical analysis. AntB and NS provided support and advice in dataset retrieval and normalization. SF-R performed the histochemical stainings. PS-M and SF-R performed genotyping analyses. XL and JWL contributed to the experimental design and executed the metabolomic analyses. GM and PPi performed to the biochemical ATP measurement *in vitro* and mitochondria analysis. GV, PZ-G and ML performed or coordinated (GV) subcutaneous xenograft experiments. JU, AnnB, MGu and RRG performed or coordinated (RRG) the intra-cardiac and intra-tibial metastasis assays. RRG contributed to the design of the patient gene signature analysis. MGr carried out microvessel staining and quantifications. PPa and VS-M provided technical advice and contributed to *in vitro* analysis. NM-M, AA-A and AZ-L contributed to the experimental design and discussion. AC-M and NE performed Seahorse assays. JDS and RB performed or coordinated (RB) the cloning of *Pgc1a* in lentiviral vectors. CCC and MC carried out the pathological analysis and scoring of the xenografts and GEMMs. AU-O, IL-V, AL-I and MU-U provided BPH and PCa samples for gene expression analysis from Basurto University Hospital. AMA contributed to the discussion of the results. AC directed the project, contributed to data analysis and wrote the manuscript.

Accession numbers and datasets

Primary accessions: The transcriptomic data generated in this publication have been deposited in NCBI's Gene Expression Omnibus and are accessible through GEO Series accession number GSE75193 (https://www.ncbi.nlm.nih.gov/geo/query/acc.cgi?acc=GSE75193)

Referenced accessions: Grasso *et* al., GEO: GSE35988; Lapointe *et* al., GEO: GSE3933; Taylor *et* al., GEO: GSE21032; Tomlins *et* al., GEO: GSE6099; Varambally *et* al., GEO: GSE3325.

[6]Dept. of Morphology, Surgery and Experimental Medicine, Section of Pathology, Oncology and Experimental Biology, University of Ferrara, Italy

[7]Vascular Signalling Laboratory, Institut d'Investigació Biomèdica de Bellvitge (IDIBELL), Gran Via de l'Hospitalet 199-203, 08907 L'Hospitalet de Llobregat, Barcelona, Spain

[8]Tumour Plasticity Team, Randall Division of Cell and Molecular Biophysics, King's College London, New Hunt's House, Guy's Campus, London SE1 1UL, UK

[9]Department of Biochemistry and Molecular Biology I, School of Biology, Complutense University and Instituto de Investigaciones Sanitarias San Carlos (IdISSC) 28040 Madrid, Spain

[10]Biostatistics / Bioinformatics Unit, - IRB Barcelona, Parc Científic de Barcelona, 08028 Barcelona, Spain

[11]Department of Pathology, Basurto University Hospital, 48013 Bilbao, Spain

[12]Department of Urology, Basurto University Hospital, 48013 Bilbao, Spain

[13]Computational Biology, Memorial Sloan-Kettering Cancer Center, NY, 10065, USA

[14]Centro de Investigación Biomédica en Red de Enfermedades Hepáticas y Digestivas (CIBERehd)

[15]Institució Catalana de Recerca i Estudis Avançats (ICREA), 08010 Barcelona, Spain

[16]Ikerbasque, Basque foundation for science, 48011 Bilbao, Spain

[17]Biochemistry and Molecular Biology Department, University of the Basque Country (UPV/EHU), P. O. Box 644, E-48080 Bilbao, Spain.

[#] These authors contributed equally to this work.

Abstract

Cellular transformation and cancer progression is accompanied by changes in the metabolic landscape. Master co-regulators of metabolism orchestrate the modulation of multiple metabolic pathways through transcriptional programs, and hence constitute a probabilistically parsimonious mechanism for general metabolic rewiring. Here we show that the transcriptional co-activator PGC1α suppresses prostate cancer progression and metastasis. A metabolic co-regulator data mining analysis unveiled that PGC1α is down-regulated in prostate cancer and associated to disease progression. Using genetically engineered mouse models and xenografts, we demonstrated that PGC1α opposes prostate cancer progression and metastasis. Mechanistically, the use of integrative metabolomics and transcriptomics revealed that PGC1α activates an Oestrogen-related receptor alpha (ERRα)-dependent transcriptional program to elicit a catabolic state and metastasis suppression. Importantly, a signature based on the PGC1α-ERRα pathway exhibited prognostic potential in prostate cancer, thus uncovering the relevance of monitoring and manipulating this pathway for prostate cancer stratification and treatment.

The metabolic switch in cancer encompasses a plethora of discrete enzymatic activities that must be coordinately altered in order to ensure the generation of biomass, reductive power and the remodelling of the microenvironment[1-4]. Despite the existence of mutations in

metabolic enzymes[5], it is widely accepted that the main trigger for metabolic reprogramming is the alteration in cancer genes that remodel the signalling landscape[2]. Numerous reports provide evidence of the pathways regulating one or a few enzymes within a metabolic pathway in cancer. However, the means of coordinated regulation of complex metabolic networks remain poorly documented.

Master transcriptional co-regulators of metabolism control a variety of genes that are in charge of remodelling the metabolic landscape, and their impact in cellular and systemic physiology has been studied for decades. It is worth noting that these co-regulators, through their capacity to interact and regulate diverse transcription factors, exhibit a unique capacity to control complex and extensive transcriptional networks, making them ideal candidates to promote or oppose oncogenic metabolic programs.

The tumour suppressor PTEN is a negative regulator of cell growth, transformation and metabolism[6-9]. PTEN and its main downstream pathway, PI-3-Kinase, have been extensively implicated in prostate cancer (PCa) pathogenesis and progression[10-12]. This tumour suppressor is progressively lost through the progression of PCa, and complete loss of PTEN is predominant in advanced disease and metastasis[8]. Genetically engineered mouse models (GEMMs) recapitulate many of the features of PCa progression. However, the molecular and metabolic bases for PCa metastasis remain poorly understood[13-16]. Indeed, complete loss of PTEN in the mouse prostate does not result in metastasis[11], in turn suggesting that additional critical events are required in this process.

In this study, we designed a bioinformatics analysis to interrogate multiple PCa datasets encompassing hundreds of well-annotated specimens. This approach allowed us to define a master regulator of PCa metabolism that is crucial for the progression of the disease. Our results identify the Peroxisome proliferator-activated receptor gamma co-activator 1 alpha (PGC1α) as a suppressor of PCa metastasis. This transcriptional co-activator exerts its function through the regulation of Oestrogen-related receptor alpha (ERRα) activity, in concordance with the activation of a catabolic program and the inhibition of PCa metastasis.

Results

A bioinformatics screen identifies *PGC1A* as metabolic co-regulator associated to prostate cancer progression

We approached the study of PCa metabolism applying criteria to ensure the selection of relevant master regulators that contribute to the metabolic switch. We focused on transcriptional co-regulators of metabolism[17] that i) were consistently altered in several publicly available PCa datasets[18-24], and ii) were associated with reduced time to recurrence and disease aggressiveness. We first evaluated the expression levels of the metabolic co-regulators in a study comprising 150 PCa specimens and 29 non-pathological prostate tissues (or controls)[22]. The analysis revealed 10 co-regulators in the set of study with significant differential expression in PCa compared to non-neoplastic prostate tissue (**Fig. 1a, Supplementary Fig. 1A**). We next extended this observation to four additional datasets[18,21,23,24] in which there was available data for non-tumoural and PCa tissues. Only the alteration in *PPARGC1A* (*PGC1A*), *PPARGC1B* (*PGC1B*) and *HDAC1* expression was

further confirmed in the majority or all sets (**Fig. 1b, Supplementary Fig. 1B**). Among these, *PGC1A* was the sole co-regulator with altered expression associated to Gleason score (**Supplementary Fig. 1C, D**) and DFS (**Fig. 1c**).

In order to rule out that cellular proliferation could contribute to the alteration of metabolic regulators, we carried out an additional analysis in which we compared the expression of *PGC1A* in PCa *versus* a benign hyper-proliferative condition (benign prostate hyperplasia or BPH). The results corroborated that the decrease in *PGC1A* expression is associated to a cancerous state rather than to a proliferative condition (**Supplementary Fig. 1E**).

We observed that the expression of *PGC1A* was progressively decreased from primary tumours to metastasis (**Fig. 1d, Supplementary Fig. 1F**). Strikingly, genomic analysis revealed shallow deletions of *PGC1A* exquisitely restricted to metastatic PCa specimens[19-22,25] (**Fig. 1e**), in full agreement with the notion that there is a selective pressure to reduce the expression of this transcriptional co-activator as the disease progresses.

From our analysis, PGC1α emerges as the major master metabolic co-regulator altered in PCa, with an expression pattern reminiscent of a tumour suppressor.

Pgc1a deletion in the murine prostate epithelium promotes prostate cancer metastasis

PGC1α has been widely studied in the context of systemic metabolism[26], whereas its activity in cancer is just beginning to be understood[27-33]. To ascertain the role of PGC1α in PCa *in vivo*, we conditionally deleted this metabolic co-regulator in the prostate epithelium[34], alone or in combination with loss of the tumour suppressor *Pten*[11] (**Fig. 2a-d, Supplementary Fig. 2A, B**). *Pgc1a* deletion alone or in the context of *Pten* heterozygosity did not result in any differential tissue mass or histological alteration, which led us to conclude that it is not an initiating event (**Fig. 2b, d**). However, compound loss of both *Pten* and *Pgc1a* resulted in significantly larger prostate mass (**Fig. 2c**), together with a remarkable increase in the rate of invasive cancer (**Fig. 2d**). Histological analysis of the prostate revealed the existence of vascular invasion in double mutant mice (DKO), but not in *Pten*-deleted (*Pten* KO) prostates (**Supplementary Fig. 2C**). PGC1α regulates the inflammatory response, which could influence and contribute to the phenotype observed[35]. However, we did not observe significant differences in the infiltration of polimorphonuclear netrophils (PMN) and lympho-plasmacytic infiltrates in our experimental settings (**Supplementary Fig. 2D**). PGC1α has been also shown to induce angiogenesis in coherence with the induction of VEGF-A expression[36]. *Pgc1a* status in our GEMM did not alter VEGF-A expression and microvessel density (**Supplementary Fig. 2E, F)**. We therefore excluded the possibility that regulation of angiogenesis or inflammation downstream PGC1α could drive the phenotype characterised in this study.

PCa GEMMs faithfully recapitulate many of the features of the human disease[37]. A reduced number of mouse models with clinically relevant mutations show increased metastatic potential[13-16]. Strikingly, histopathological analysis of our mouse model in the context of *Pten* loss revealed that DKO mice - but not *Pten* KO counterparts - presented evidence of metastasis, which was estimated in 44% to lymph nodes (LN) and 20% to liver (**Fig. 2e, f**

and Supplementary Fig. 2G). Metastatic dissemination was in agreement with the observation of Pan-cytokeratin (PanCK) and Androgen Receptor (AR)-positive PCa cell deposits in the lymph nodes of DKO mice (**Fig. 2g).** Of note, 33% of *Pten* KO mice presented small groups of PanCK-positive cells in LN (without metastatic lesions) (**Supplementary Fig. 2H**), suggesting that even if these cells are able to reach the LN, they lack capacity to establish clinical metastasis. Interestingly, bone analysis revealed disseminated groups (but not clinical metastasis) of PanCK-positive cells in DKO but not in *Pten* KO mice **(Supplementary Fig. 2I-K**). Analysis of a small cohort of $Pten^{pc-/-}$; $Pgc1a^{pc+/-}$ mice demonstrated that heterozygous loss of *Pgc1a* is sufficient to promote aggressiveness, vascular invasion and metastasis (**Supplementary Fig. 2L-N**). This observation supports the notion that single copy loss of *PGC1A* (as observed in metastatic human PCa specimens, **Fig. 1e**) could be a key contributing factor to the metastatic phenotype.

The cooperative effect observed in our mouse model between loss of *Pten* and *Pgc1a* was supported by the direct correlation of the two transcripts in patient specimens and the association of *PGC1A* down-regulation with *PTEN* genomic loss (TCGA provisional data[19,20], **Supplementary Fig. 2O**).

In summary, our data in GEMMs and patient datasets formally demonstrates that the down-regulation of PGC1α in PCa is an unprecedented causal event for the progression of the disease and its metastatic dissemination.

PGC1α suppresses prostate cancer growth and metastasis

In order to characterize the prostate tumour suppressive activity of PGC1α, we first evaluated its expression level in well-established PCa cell lines[38]. Using previously reported PGC1α-positive and negative melanoma cells[28], we could demonstrate that PCa cell lines lack detectable expression of the transcriptional co-activator at the protein level (**Fig. 3a**). In agreement with this notion, PGC1α-silencing in these cells failed to impact on the expression of its well-established targets[39] (**Supplementary Fig. 3A**). Importantly, through the analysis of publicly available datasets[22], we could demonstrate that the transcript levels of *PGC1A* in metastatic cell lines are comparable to those observed in human metastatic PCa specimens and vastly reduced compared to PGC1α-positive melanoma cells (**Fig. 3a, Supplementary Fig. 3B**). Despite our efforts to optimize the detection of the protein with different commercial antibodies, we could not identify an immunoreactive band that would correspond to PGC1α, in contrast with other reports[40,41]. Yet, we cannot rule out that in non-basal conditions, stimulation of other factors such as AR[41] or AMPK[40] could lead to the up-regulation and allow detection of PGC1α in PCa cells.

Due to the lack of PGC1α detection in PCa cellular systems, we aimed at reconstituting the expression of this gene to levels achievable in the cancer cell lines previously reported[28]. By means of lentiviral delivery of inducible Pgc1α and doxycycline titration, we reached expression levels of this protein in three PCa cell lines (AR-dependent - LnCaP - and independent - PC3 and DU145) equivalent to that observed in the PGC1α-expressing melanoma cell line MeWo (**Fig. 3b, Supplementary Fig. 3C, D**). Next, we evaluated the

cellular outcome of expressing PGC1α in PCa cell lines. Interestingly, expression of Pgc1α in this context resulted in a reduction in bi-dimensional and three-dimensional growth (**Fig. 3c, d, Supplementary Fig. E**), cellular proliferation (**Fig. 3e, Supplementary Fig. 3F**) and cell cycle progression (**Supplementary Fig. 3G**). Of note, we excluded the possibility that doxycycline treatment could influence the result of the growth analysis (**Supplementary Fig. 3H**). The Pgc1α phenotype was recapitulated *in vivo*, where ectopic expression of this gene decreased tumour formation and growth (**Fig. 3f, Supplementary Fig. 3I-K**). In agreement with the GEMM data, we did not observe a contribution of angiogenesis to the phenotype (**Supplementary Fig. 3L-N**).

We observed in GEMMs that *Pgc1a*-loss resulted in metastatic dissemination **(Fig. 2)**. We next sought to study whether Pgc1α expression could oppose a pre-existing metastatic phenotype. To this end, we carried out xenotransplant assays in immunocompromised mice using luciferase-expressing Pgc1α-inducible PC3 cells. Intra-cardiac injection of these cells (**Fig. 3g**) revealed that Pgc1α expression blunted metastatic growth in the lung, and led to a remarkable decrease in bone colonisation (**Fig. 3h-i**). As an additional approach, we sought to analyse metastatic tumour re-initiation capacity by means of local injection of PCa cells at the metastatic site. Since PCa exhibits osteotropic nature[42], we carried out intra-tibial injection of cells and the appearance of tumour masses in the bone was monitored[43] (**Fig. 3j**). The results demonstrated that PGC1α exerts a potent anti-metastatic activity both in bone tumour mass and metastatic foci (**Fig. 3k**). These data provide evidence of the anti-metastatic potential of PGC1α.

PGC1α determines the oncogenic metabolic wiring in prostate cancer

PGC1α regulates gene expression through the interaction with diverse transcription factors[26]. In order to define the transcriptional program associated to the tumour suppressive activity of PGC1α, we performed gene expression profiling from Pgc1α-expressing *vs.* non-expressing PC3 cells. We identified 174 probes with significantly altered signal encoding genes predominantly related to functions such as mitochondrial catabolic programs and energy-producing processes[26,44] (**Supplementary Table 1, Fig. 4a**), which we validated by qRTPCR (**Fig. 4b-d, Supplementary Fig. 4**).

In order to demonstrate that the tumour suppressive activity of PGC1α was indeed accompanied by a global metabolic wiring, we carried out integrative metabolomics. We analysed cell line, xenograft and GEMM tissue extracts using liquid-chromatography high-resolution mass spectrometry (LC-HRMS). LC-HRMS metabolomics and subsequent biochemical assays confirmed that oxidative processes such as fatty acid β-oxidation (Fig. 5a-d, Supplementary Fig. 5A-C, Supplementary Table 2-5) and tricarboxylic acid cycle (TCA, **Fig. 5e, Supplementary Fig. 5D**) were increased in response to Pgc1α expression. In order to quantitatively define the use of glucose in the TCA cycle, we carried out stable ^{13}C-U_6-Glucose isotope labelling. This experimental approach provided definitive evidence of the increased oxidation of glucose in the mitochondria in Pgc1α expressing cells (**Fig. 5f**). This metabolic wiring was consistent with elevated oxygen consumption (basal and ATP-producing) and ATP levels upon Pgc1α expression (Fig. 5g-i, Supplementary Fig. 5E-I, Supplementary Tables S2-5).

We next reasoned that over-activation of mitochondrial oxidative processes would lead to decreased anabolic routes. On the one hand, we monitored the incorporation of carbons from ^{13}C-U_6-Glucose into fatty acids (through the export of citrate from TCA to the cytoplasm[45] and conversion to acetyl CoA that is used for *de novo* lipid synthesis). Interestingly, we found a significant decrease in ^{13}C incorporation into palmitate (reflected as ^{13}C carbon pairs) when Pgc1α was expressed (**Fig. 5j, Supplementary Fig. 5J)**. On the other hand, we monitored lactate production as a readout of aerobic glycolysis or "the Warburg effect"[2], which has been associated to the anabolic switch. As predicted, Pgc1α-expressing cells exhibited reduced extracellular lactate levels (**Supplementary Fig. 5K**). Of note, lactate production and respiration were unaltered by doxycycline challenge in non-transduced PC3 cells (**Supplementary Fig. 5L, M**). Taken together, our data provide a metabolic basis for the tumour suppressive potential of PGC1α in PCa, according to which this metabolic co-regulator controls the balance between catabolic and anabolic processes (**Fig. 5k**).

An ERRα-dependent transcriptional program mediates the prostate tumour suppressive activity of PGC1α

We next aimed to identify the transcription factor that mediated the activity of PGC1α, and hence we performed a promoter enrichment analysis. The results revealed a predominant abundance in genes regulated by ERRα (**Fig. 6a**). We corroborated these results with Gene Set Enrichment Analysis (GSEA; Normalized Enrichment Score=2.02; Nominal p value=0.0109)[46]. This transcription factor controls a wide array of metabolic functions, from oxidative processes to mitochondrial biogenesis[44]. We have shown that PGC1α is indeed capable of regulating functions attributed to ERRα, such as mitochondrial oxidative metabolism (**Fig. 4, 5 and Supplementary Fig. 4, 5**). In addition, we observed that Pgc1a expression led to increased mitochondrial volume (**Supplementary Fig. 6A**). In order to ascertain to which extent the growth inhibitory and anti-metastatic activity of PGC1α required its ability to interact with ERRα, we took advantage of a mutant variant of the co-activator ($PGC1\alpha^{L2L3M}$) that is unable to interact with this and other nuclear receptors[46,47]. The expression of $PGC1\alpha^{L2L3M}$ in PC3 cells (**Supplementary Fig. 6B**) failed to up-regulate target genes, to reprogram oxidative metabolism, to inhibit cell growth, and, importantly, to suppress bone metastasis in intratibial xenografts (**Fig. 6b-f, Supplementary Fig. 6C**). To further discriminate between PGC1a functions that depend on ERRa or other nuclear receptors, we undertook a targeted silencing approach, and we transduced Pgc1α-inducible PC3 cells with an ERRα-targeting or a scramble shRNA (**Supplementary Fig. 6D**). In coherence with the L2L3M mutant data, ERRα silencing partially blunted the effects of Pgc1α on gene expression and cell growth (**Fig. 6g, Supplementary Fig. 6H)**. *In vivo*, silencing of ERRα in the presence of the ectopically expressed transcriptional co-activator resulted in a significant increase in bone metastasis incidence from 40% (in Pgc1α-expressing cells transduced with scramble shRNA) to full penetrance (**Fig. 6h**). Of note, the requirement of ERRα for the effect of PGC1α was recapitulated *in vitro* with a reverse agonist of the transcription factor, namely XCT790[48] (**Supplementary Fig. 6F-I**).

It is worth noting that other metabolic pathways have been suggested to sustain the metastatic phenotype. Oxidative stress has been shown to limit metastatic potential in breast

cancer and melanoma[29,49]. PGC1α regulates the expression of antioxidant genes, while the enhancement of mitochondrial metabolism can lead to the production of reactive oxygen species (ROS)[28,29,49] (**Fig. 4b and Supplementary Table 1**). We therefore tested whether ROS production was modified in our experimental settings and if it could contribute to the phenotype observed. Mitochondrial and cellular ROS production were not consistently altered by Pgc1α expression *in vitro* (**Supplementary Fig. 6J**). In addition, lipid peroxidation (which serves as readout of ROS production) was unaffected in our xenograft study (**Supplementary Fig. 6K**). These results are coherent with the inability of antioxidants to rescue the proliferative defect elicited by Pgc1α (**Supplementary Fig. 6L**).

Our data provides a molecular mechanism by which ERRα activation downstream PGC1α promotes a metabolic rewiring that suppresses PCa proliferation and metastasis.

A PGC1α-ERRα transcriptional signature harbours prognostic potential

We have shown that reduced *PGC1A* expression in PCa exhibits prognostic potential (**Fig. 1c**). Since our data demonstrates that transcriptional regulation downstream ERRα is key for the tumour suppressive activity of this co-activator, we reasoned that the association of PGC1α with aggressiveness and DFS should be recapitulated when monitoring ERRα target genes (**Fig. 7a**). We started the analysis from the list of genes positively regulated by PGC1α in our cellular system (153 genes, **Fig. 7b**). As predicted, the analysis in two independent patient datasets confirmed that the average signal of the PGC1α gene list was positively correlated with time to PCa recurrence (**Fig. 7c**). In addition, we observed a decrease in the expression of the aforementioned gene list associated to disease initiation and progression (**Supplementary Fig. 7A**). Importantly, comparable results were obtained when we performed the analysis with the subset of ERRα-target genes within the PGC1α gene set (73 genes, **Supplementary Table 6**, **Fig. 7b, d and Supplementary Fig. 7B**). We next sought to curate the gene list in order to consolidate a prognostic PGC1α-ERRα gene set. We therefore focused on genes that exhibited a strong correlation with *PGC1A* in patient datasets. We selected genes that were significantly correlated with the co-activator ($R>0.2$; $p<0.05$) in at least 3 out of 5 studies. The results unveiled a PGC1α transcriptional signature in patients consisting of 17 genes, the majority of which i) were directly correlated with the transcriptional co-activator in the queried datasets, ii) exhibited decreased expression in PCa *vs.* BPH and iii) were further down-regulated in metastatic disease (**Supplementary Table 7, Supplementary Fig. 7C, D**). Nearly 60% of these genes were regulated by ERRα (10 genes out of 17) and were selected for further analysis as a *PGC1α-ERRα curated gene set* (**Supplementary Table 7**). The results revealed reduced *PGC1α-ERRα curated gene set* expression as the disease progressed (**Fig. 7e**). We next analysed the association of the *PGC1α-ERRα curated gene set* with disease recurrence. To this end, we compared patients harbouring primary tumours with signal values in the first quartile (Q1) *versus* the rest (Q2-Q4). Patients with signature positive tumours exhibited reduced DFS in two independent datasets (**Fig. 7f**). A Hazard ratio (HR) of 4.2 (Taylor) and 17.8 (TCGA) was defined for signature-positive patients, while signature-negative individuals presented reduced risk of recurrence, with HR of 0.23 (Taylor) and 0.05 (TCGA). Furthermore, the frequency of patients with signature-positive signal values was absent or low in the normal prostate group and further increased in metastasis compared to primary tumours (**Supplementary Fig. 7E**).

Taken together, ERRα-regulated metabolic transcriptional program is associated to the activity of PGC1α in PCa. This interplay is conserved in patient specimens and defines a gene signature that harbours prognostic potential.

Discussion

In this study we provide a comprehensive analysis of master transcriptional co-regulators of metabolism in PCa. Through the use of human data mining analysis, GEMMs and cellular systems, our study presents evidence demonstrating that PGC1α exerts a tumour suppressive activity opposing PCa metastasis. Interestingly, three out of ten significantly altered co-regulators (*PGC1A*, *PGC1B* and *NRIP1*, **Fig. 1a**) in the *Taylor*[22] PCa dataset (2 out of 3 consistently altered throughout databases, **Fig. 1b**) converge in the regulation of a common transcriptional metabolic program, led by ERRα[44] and that is associated to the phenotype observed in this study. These data strongly suggest that such pathway is of critical importance for the control of aggressiveness properties in PCa. Indeed, our results demonstrate that a gene set composed of ERRα target genes that are under the control of PGC1α expression 1) is progressively down-regulated in PCa and metastatic disease, and 2) presents prognostic potential for the identification of patients at risk of early recurrence.

The study of the tumour suppressive potential of Pgc1α in mouse models allowed us to characterise a clinically relevant PCa GEMM presenting enhanced metastatic dissemination. PGC1α is added to the short list of genetic events that drive metastasis in this model[13-16], and the first to be explicitly linked to the regulation of the metabolic switch. Overall, our finding is of importance for the future study of the requirements for PCa metastasis and therefore for therapeutic purposes.

The sole alteration of PGC1α expression in PCa has profound impact on the oncogenic metabolic switch[50]. This data is in line with the reported activities of this protein in metabolism and mitochondrial biogenesis[26]. Of note, despite the widely accepted fact that the reported metabolic switch[50] has comparable consequences in all cancer scenarios, the study of PGC1α in other tumour types has also revealed a selective pressure towards oxidative processes[27-29]. Previous work from others and us defined PGC1α signalling as a selective advantage for breast cancer and melanoma cells[4,27-29,51]. The contribution of this co-activator to cellular proliferation differs between tumour types and experimental systems, promoting growth in melanoma[28] while irrelevant to breast cancer cells[29]. Interestingly, in breast circulating tumour cells, PGC1α expression supports metastatic capacity[29]. The molecular pathways regulating these diverse biological features converge in the activation of ERRα and Peroxisome proliferator-activated receptors (PPAR). While PPAR activation mediates the increase in fatty acid β-oxidation[4], ERRα is responsible for the overall increase in oxidative metabolism and mitochondrial biogenesis[44]. Similarly, the activation of an antioxidant transcriptional program has been suggested to contribute to anoikis and cancer cell dissemination in a PGC1α-dependent and independent manner[27,28,49,52]. In PCa, however, we demonstrate that the oxidative metabolic program elicited by PGC1α prevents tumour growth and metastatic dissemination, in the absence of overt changes in ROS production, inflammatory response or angiogenic signals. These findings support the notion that the optimal metabolic wiring for tumour growth and metastasis might differ depending

on the tumour type, the mutational landscape of the tumour and, potentially, the microenvironment. This would lead to opposite activities of PGC1α depending on the cancer setting, from metastatic promoter[29] to metastasis suppressor (as we demonstrate in the present work).

In summary, our study identifies PGC1α as a master regulator of PCa metabolism that opposes the dissemination of the disease. Therefore, a PGC1α-regulated ERRα-dependent transcriptional program might open new avenues in the identification of metabolic transcriptional signatures that can be exploited for patient stratification and the use of metabolism-modulatory therapies.

Materials and Methods

Reagents

3-[4-(2,4-Bis-trifluoromethylbenzyloxy)-3-methoxyphenyl]-2-cyano-N-(5-trifluoromethyl-1,3,4-thiadiazol-2-yl)acrylamide (XCT 790), etomoxir (ETO), Doxycycline hyclate (Dox), oligomycin, N-acetyl-cysteine (NAC) and Manganese (III) tetrakis (4-benzoic acid)porphyrin chloride (MnTBAP) were purchased from Sigma.

Cell culture

Human prostate carcinoma cell lines, LnCaP, DU145 and PC3 were purchased from Leibniz-Institut DSMZ - Deutsche Sammlung von Mikroorganismen und Zellkulturen GmbH, who provided authentication certificate. None of the cell lines used in this study were found in the database of commonly misidentified cell lines maintained by ICLAC and NCBI Biosample. Cells were transduced with a modified TRIPZ (Dharmacon) doxycycline inducible lentiviral construct in which the RFP and miR30 region was substituted by *HA-Flag-Pgc1a*[51] or *HA-Flag-Pgc1a*^{L2L3M} [47]. Lentiviral shRNA constructs targeting *PGC1A* (TRCN0000001166) and *ESRRA* (TRCN0000022180) where purchased in Sigma and a scramble shRNA (hairpin sequence: CCGGCAACAAGATGAAGAGCACCAACTCGAGTTGGTGCTCTTCATCTTGTTG) was used as control. For *ESRRA* shRNAs, Puromycin resistance cassette was replaced by Hygromycin cassette from pLKO.1 Hygro (Addgene Ref. 24150) using BamHI and KpnI sites. Melanoma lines were kindly provided by Dr. Boyano[53] and Dr. Buque and purchased from ATCC. Cell lines were routinely monitored for mycoplasma contamination and quarantined while treated if positive.

Animals

All mouse experiments were carried out following the ethical guidelines established by the Biosafety and Welfare Committee at CIC bioGUNE and The Institutional Animal Care and Use Committee of IRB Barcelona. The procedures employed were carried out following the recommendations from AAALAC. Xenograft experiments were performed as previously described[54], injecting 10^6 cells per condition in two flanks per mouse. PC3 TRIPZ-HA-Pgc1a cells were injected in each flank of nude mice and 24 h post-injections mice were fed with chow or doxycycline diet (Research diets, D12100402). GEMM experiments were carried out as reported in a mixed background[11,14,55,56] (where the founder colony was

cross-bred for at least three generations prior to the expansion of experimental cohorts in order to ensure and homogenous mixed background). The *Pten*^{loxP} and *Pgc1a*^{loxP} conditional knockout alleles have been described elsewhere[11,34]. Prostate epithelium specific deletion was effected by the Pb-*Cre4*[11]. Mice were fasted for 6 h prior to tissue harvest (9 am-3 pm) in order to prevent metabolic alterations due to immediate food intake.

For intra-tibial and intra-cardiac injections BALB/c nude male mice (Harlan) of 9-11 weeks of age were used. Before the injections, PC3 Tripz-HA-Pgc1a (WT, L2L3M, shSC, shERRA) cell lines were pre-treated for 48h with PBS or doxycycline (0.5μg/ml). Mice injected with cells treated with doxycycline were also pre-treated for 48h with 1mg/ml of doxycycline in drinking water. After the injections this group of mice was left on continuous doxycycline treatment (1mg/ml in drinking water). Before the injections mice were anesthetized with mixture of Kethamine (80 mg/kg) and Xilacine (8 mg/kg). For intra-tibial injections, 1×10^4 cells were resuspended in final volume of 5 μl of cold PBS and injected as described previously[57]. For intra-cardiac injections 2×10^5 cells were resuspended in final volume of 100 μl of cold PBS and injected as described previously[57]. Upon the injections tumour development was followed on weekly basis by BLI using the IVIS-200 imaging system from Xenogen. Quantification of bioluminescent images was done with Living Image 2.60.1 software. the development of metastasis was confirmed by doing *in vivo* or *ex vivo* (upon necropsy) bioluminescent images of organs of interest (metastasis positivity in lesion incidence analysis was defined as tibias with luciferase signals greater than 50.000 units). When comparing cell lines independently transduced with the luciferase-expressing vector (Fig. 6h), photon flux values per limb where presented as normalized signal (corrected by basal signal, obtained within 24 hours after injection): Normalized photon flux = [day 14 signal/day 0 signal] × 1000. For metastasis-free survival curves metastatic event was scored when measured value of bioluminescence bypasses 1/10 of the day 0 value.

Patient samples

All samples were obtained from the Basque Biobank for research (BIOEF, Basurto University hospital) upon informed consent and with evaluation and approval from the corresponding ethics committee (CEIC code OHEUN11-12 and OHEUN14-14).

Cellular, molecular and metabolic assays

Cell number quantification with crystal violet[58] was performed as referenced.

Western blot was performed as previously described[51]. Antibodies used: PGC1α (H300; Santa Cruz Biotechnology sc-13067; dilution 1:1000); ERRα (E1G1J; Cell Signalling #13826; dilution 1:1000); β-Actin (clone AC-74; Sigma #A 5316; dilution 1:2000); GAPDH (clone 14C10; Cell Signalling #2218; dilution 1:1000); HSP90 (Cell Signalling; #4874; dilution 1:1000).

RNA was extracted using NucleoSpin® RNA isolation kit from Macherey-Nagel (ref: 740955.240C). For patients and animal tissues a Trizol-based implementation of the NucleoSpin® RNA isolation kit protocol was used as reported[59]. For all cases, 1μg of total RNA was used for cDNA synthesis using qScript cDNA Supermix from Quanta (ref. 95048). Quantitative Real Time PCR (qRTPCR) was performed as previously described[51].

Universal Probe Library (Roche) primers and probes employed are detailed in Supplementary Table 8. β-ACTIN (Hs99999903_m1; Mm0607939_s1) and GAPDH (Hs02758991_g1, Mm99999915_g1) housekeeping assays from Applied Biosystems showed similar results (all qRTPCR data presented was normalized using GAPDH/Gapdh).

FAO was performed as previously described[51]. Lactate production was performed as referenced[60] using Trinity Biotech lactate measurement kit.

Oxygen consumption rate (OCR) was measured with a XF24 extracellular flux analyser (Seahorse Bioscience)[61]. Briefly, 50.000 cells per well were seeded in a XF24 plate, and OCR measurements were normalized to cell number analysed by crystal violet. Cells were initially plated in 10% FBS DMEM media for 24 hours, and 1h before measurements, media was changed to DMEM serum and bicarbonate free, with glutamine and glucose (10mM). Mitochondrial stress test was carried out using the following concentrations of injected compound: Oligomycin (1μM).

For mitochondrial ATP assays, 50.000 PC3 and DU145 cells plated onto 13-mm coverslips and transfected with a mitochondrial targeted luciferase chimera (mtLuc). Cells were perfused in the luminometer at 37°C with KRB solution containing 25 μM luciferin and 1 mM $CaCl_2$ and supplemented with 5.5 mM glucose. Under these conditions, the light output of a coverslip of transfected cells was in the range of 5.000–20.000 cps for the luciferase construct vs. a background lower than 100 cps. Luminescence was entirely dependent on the presence of luciferin and was proportional to the perfused luciferin concentration between 20 and 200 μM.

Mitochondrial morphology was assessed by using a cDNA encoding mitochondrial matrix-targeted DsRed (mtDsRed). Cells were seeded onto 24-mm diameter coverslip (thickness between 0.16–0.19 mm) (Thermo Scientific) and 24 h later cells were transfected with 2μg mtDSred (Lipofectamine LTX reagent; Invitrogen). mtDsRed expression was assessed 36 h later. All the acquisitions were performed with a confocal Nikon Eclipse T_i system and fluorescent images were captured by using NisElements 3.2.

Lipid peroxidation based on MDA detection was assayed in xenograft samples following the manufacture instructions (MAK085 Sigma-Aldrich).

ROS production was determined by Mitosox and DCF staining as previously described[62].

Histopathological analysis

After euthanasia, histological evaluation of a Haematoxylin and eosin (H&E) stained section from formalin-fixed paraffin embedded tissues of the following organs was performed: prostate gland, lymph nodes, long bones from lower limbs and other solid organs such as lungs and liver.

Following the consensus reported by Ittmann et al.[63], prostate gland alterations were classified into 4 categories: gland within normal limits; high grade prostatic intraepithelial neoplasia (HGPIN); HGPIN with focal micro-invasion; and invasive carcinoma.

Lymphovascular invasion was assessed in all cases were micro-invasion foci or invasive carcinoma were observed.

Lymph node (LN) metastasis and the presence of groups of PCa cells in bone marrow (BM) were determined after haematoxylin-eosin (H&E) staining (LN) and immunohistochemical identification of cytokeratin (CK) and androgen receptor (AR) -expressing cells using a pan-CK rabbit polyclonal antibody (Dako, Carpinteria, CA) and AR rabbit polyclonal antibody (Santa Cruz Biotechnology, sc-816) (LN and BM). In the case of BM, cases were classified as “dissemination negative” when none or few scattered (less than 5) CK-expressing cells were identified and “dissemination positive” when more than 5 or small groups of these cells were observed.

To assess the inflammatory component in the prostate tissues we performed a semi-quantitative analysis in the glandular and the stromal areas separately for each of the specimens. We first determined the type of inflammatory cell present in each tissue compartment: polymorphonuclear neutrophils versus lympho-plasmacytic infiltrates. Then we performed a quantification of these cells using the following score system: 0- no inflammatory cells, 1-few cells, 2-moderate amount of cells and 3-high amount of cells. Scores in between were also determined as 0.5, 1.5 and 2.5. If both types of cells were present in one compartment, we chose the highest as the final score.

Proliferation was assessed in paraffin embedded xenografts samples by using Ki67 antibody (MA5-14520, Thermo Scientific). Microvessel density was determined and quantified in GEMMs and xenograft samples by the immunodetection of CD31 (Rabbit anti-CD31; Ref. ab28364 Abcam).

Metabolomics

LCHR-MS metabolomics and stable isotope ^{13}C-U$_6$-Glucose labelling was performed as reported[64-66]. Briefly, PC3 TRIPZ-HA-Flag-Pgc1a cells treated or untreated for 72h with 0.5μg/ml doxycycline were plated at 500.000 cells/well in 6-well plates. For LCHR-MS metabolomics and grown maintaining the doxycycline regime for 42h before harvesting, while for stable isotope ^{13}C-U$_6$-Glucose labelling experiments, 24h after seeding cells were washed and exposed to media with serum, without glucose and pyruvate and supplemented 2mM ^{13}C-U$_6$-Glucose. 16h after that, cells were washed and another ^{13}C-U$_6$-Glucose pulse was performed for 2h before harvesting.

Transcriptomic analysis

For transcriptomic analysis in PC3 TRIPZ-HA-Flag-Pgc1α cells, Illumina whole genome - HumanHT-12_V4.0 (DirHyb, nt) method was used as reported[67].

Promoter enrichment analysis was assessed with the Transcription Factors (TFs) dataset from MSigDB (The Molecular Signature Database; http://www.broadinstitute.org/gsea/msigdb/collections.jsp). TFs dataset contain genes that share a transcription factor-binding site defined in the TRANSFAC (version 7.4, http://www.gene-regulation.com/) database. Each of these gene set was annotated by a TRANSFAC record. A hypergeometric test was used to detect enriched dataset categories.

The GSEA was performed using the GenePattern web tool from the Broad Institute (http://genepattern.broadinstitute.org). The list of PGC1α upregulated genes ranked by their fold change was uploaded and analysed against a list of ERRα target genes[46]. The number of permutations carried out were 1000 and the threshold was 0.05.

Bioinformatic analysis

Database normalization: all the datasets used for the data mining analysis were downloaded from GEO, and subjected to background correction, $\log_2$ transformation and quartile normalization. In the case of using a pre-processed dataset, this normalization was reviewed and corrected if required.

Frequency of alteration of metabolic co-regulators (Fig. 1 and Fig. S1A): expression levels of the selected co-regulators were obtained from the dataset reported by Taylor *et al*[22]. A matrix containing signal values and clinical information was prepared in order to ascertain the up- or down-regulation. We computed the relative expression of an individual gene and tumour to the expression distribution in a reference population (patients without prostate tumour or metastasis). The returned value indicates the number of standard deviations away from the mean of expression in the reference population (Z-score). Using a fold change of +2 and −2 as a threshold, we determined the number of samples from the cancer dataset that were up- or down-regulated. p-values were calculated by comparing the means of normal of cancerous biopsies.

Quartile analysis in DFS: Patients biopsies from primary tumours were organized into four quartiles according to the expression of the gene of interest in two datasets. The recurrence of the disease was selected as the event of interest. Kaplan-Meier estimator was used to perform the test as it takes into account *right-censoring*, which occurs if a patient withdraws from a study. On the plot, small vertical tick-marks indicate losses, where a patient's survival time has been right-censored. With this estimator we obtained a survival curve, a graphical representation of the occurrence of the event in the different groups, and a p-value that estimate the statistical power of the differences observed.

For *PGC1A* genomic analysis, data from prostate cancer patients with copy number alteration information in Taylor[22], Grasso[21] and Robinson[25] et al. datasets was extracted from *cbioportal.org*. Percentage of shallow deletions of primary tumours and metastatic patients was calculated separately.

Correlation analysis: Pearson correlation test was applied to analyse the relationship between paired genes. From this analysis, Pearson's coefficient (R) indicates the existing linear correlation (dependence) between two variables X and Y, giving a value between +1 and –1 (both included), where 1 is total positive correlation, 0 is no correlation, and –1 is total negative correlation. The p-value indicates the significance of this R coefficient.

Statistics and Reproducibility

No statistical method was used to predetermine sample size. The experiments were not randomized. The investigators were not blinded to allocation during experiments and outcome assessment. Unless otherwise stated, data analysed by parametric tests is

represented by the mean ± s.e.m. of pooled experiments and median ± interquartile range for experiments analysed by non-parametric tests. n values represent the number of independent experiments performed, the number of individual mice or patient specimens. For each independent *in vitro* experiment, at least three technical replicates were used (exceptions: in western blot analysis technical replicates are presented, in untargeted metabolomics two technical replicates were used and for, ^{13}C-U_6-Glucose isotope labelling one technical replicate was used) and a minimum number of three experiments were done to ensure adequate statistical power. For data mining analysis, ANOVA test was used for multi-component comparisons and Student T test for two component comparisons. In the *in vitro* experiments, normal distribution was confirmed or assumed (for n<5) and Student T test was applied for two component comparisons. For *in vivo* experiments, as well as for experimental analysis of human biopsies (from Basurto U. Hospital) a non-parametric Mann-Whitney exact test was used, without using approximate algorithms to avoid different outcomes of statistics packages[68]. To this end, we applied the formulas described[69] for small-sized groups and Graphpad Prism for large-sized groups. In the statistical analyses involving fold changes, unequal variances were assumed. For contingency analysis, Fisher exact test as used for 2-group comparison (metastasis incidence) and Chi Square when analyzing more than 2 groups (analysis of PGC1α-ERRα signature frequency in PCa human specimens). The confidence level used for all the statistical analyses was of 95% (alpha value = 0.05). Two-tail statistical analysis was applied for experimental design without predicted result, and one-tail for validation or hypothesis-driven experiments.

Supplementary Material

Refer to Web version on PubMed Central for supplementary material.

Acknowledgements

Apologies to those whose related publications were not cited due to space limitations. We would like to thank the following researchers: Dr. Bruce Spiegelman for providing the *Pgc1a*^{LoxP} mice; Drs. David Santamaría and Mariano Barbacid for technical help and advice with Doxycycline-enriched diets in xenograft experiments; Dr. Pere Puigserver for providing Pgc1α-expressing constructs; Dr. Brett Carver for help and advice with dataset analysis, Dr. Donald McDonnell for providing mutant Pgc1α^{L2L3M}-expressing constructs and Drs. Boyano and Buque for providing melanoma cell lines. The work of AC is supported by the Ramón y Cajal award, the Basque Department of Industry, Tourism and Trade (Etortek), health (2012111086) and education (PI2012-03), Marie Curie (277043), Movember, ISCIII (PI10/01484, PI13/00031), FERO VIII Fellowship and the European Research Council Starting Grant (336343). N.M-M. is supported by the Spanish Association Against Cancer (AECC). AC-M is supported by the MINECO postdoctoral program and the CIG program from the European commission (660191). A.A-A and L.V-J are supported by the Basque Government of Education. PPi is grateful to Camilla degli Scrovegni for continuous support and the work in his lab was supported by the Italian Association for Cancer Research (AIRC: IG-14442), the Italian Ministry of Education, University and Research (COFIN n. 20129JLHSY_002, FIRB n. RBAP11FXBC_002, and Futuro in Ricerca n. RBFR10EGVP_001) and Italian Ministry of Health. RB is supported by MINECO (BFU2014-52282-P, BFU2011-25986) and Basque Government (PI2012/42). The work of VS-M was supported by Cancer Research UK C33043/A12065; Royal Society RG110591. PPa was supported by King's Overseas Scholarship. Work by the group of GV group was supported by grants from the Spanish Ministry of Economy and Competitiveness/Instituto de Salud Carlos III (MINECO/ISCIII) together with the European Regional Development Fund (ERDF/FEDER): PS09/01401; PI12/02248 and PI15/00339, Fundación Mutua Madrileña and Fundació la Marató de TV3. CCC and MC were funded by NIH P01CA087497. JWL is supported by R00CA168997, R01CA193256, and R21CA201963 from the National Institutes of Health. Work in MG lab was supported by SAF2014-59950-P from MINECO (Spain), 2014-SGR-725 from the Catalan Government, from the People Programme (Marie Curie Actions) of the European Union's Seventh Framework Programme FP7/2007-2013/ (REA grant agreement 317250), and the Institute of Health Carlos III (ISC III) and the European Regional Development Fund (ERDF) under the integrated Project of Excellence no. PIE13/00022 (ONCOPROFILE). J.U. is a Juan de la Cierva Researcher (MINECO). AB is a FPI-Severo Ochoa fellowship

grantee (MINECO). RRG research support was provided by the Spanish Government (MINECO) and FEDER grant SAF2013-46196, as well as the Generalitat de Catalunya AGAUR 2014-SGR grant 535.

REFERENCES

1. Loo JM, et al. Extracellular metabolic energetics can promote cancer progression. Cell. 2015; 160:393–406. doi:10.1016/j.cell.2014.12.018. [PubMed: 25601461]
2. Vander Heiden MG, Cantley LC, Thompson CB. Understanding the Warburg effect: the metabolic requirements of cell proliferation. Science. 2009; 324:1029–1033. doi:324/5930/1029 [pii]10.1126/science.1160809. [PubMed: 19460998]
3. Vander Heiden MG, et al. Evidence for an alternative glycolytic pathway in rapidly proliferating cells. Science. 2010; 329:1492–1499. doi:329/5998/1492 [pii]10.1126/science.1188015. [PubMed: 20847263]
4. Carracedo A, Cantley LC, Pandolfi PP. Cancer metabolism: fatty acid oxidation in the limelight. Nat Rev Cancer. 2013; 13:227–232. doi:nrc3483 [pii]10.1038/nrc3483. [PubMed: 23446547]
5. Yang M, Soga T, Pollard PJ. Oncometabolites: linking altered metabolism with cancer. J Clin Invest. 2013; 123:3652–3658. doi:10.1172/JCI67228. [PubMed: 23999438]
6. Ortega-Molina A, et al. Pten positively regulates brown adipose function, energy expenditure, and longevity. Cell Metab. 2012; 15:382–394. doi:10.1016/j.cmet.2012.02.001. [PubMed: 22405073]
7. Garcia-Cao I, et al. Systemic elevation of PTEN induces a tumor-suppressive metabolic state. Cell. 2012; 149:49–62. doi:S0092-8674(12)00230-9 [pii]10.1016/j.cell.2012.02.030. [PubMed: 22401813]
8. Salmena L, Carracedo A, Pandolfi PP. Tenets of PTEN tumor suppression. Cell. 2008; 133:403–414. [PubMed: 18455982]
9. Song MS, Salmena L, Pandolfi PP. The functions and regulation of the PTEN tumour suppressor. Nat Rev Mol Cell Biol. 2012; 13:283–296. doi:10.1038/nrm3330. [PubMed: 22473468]
10. Di Cristofano A, Pesce B, Cordon-Cardo C, Pandolfi PP. Pten is essential for embryonic development and tumour suppression. Nature genetics. 1998; 19:348–355. doi:10.1038/1235. [PubMed: 9697695]
11. Chen Z, et al. Crucial role of p53-dependent cellular senescence in suppression of Pten-deficient tumorigenesis. Nature. 2005; 436:725–730. doi:nature03918 [pii]10.1038/nature03918. [PubMed: 16079851]
12. Majumder PK, et al. Prostate intraepithelial neoplasia induced by prostate restricted Akt activation: the MPAKT model. Proc Natl Acad Sci U S A. 2003; 100:7841–7846. doi:10.1073/pnas.1232229100. [PubMed: 12799464]
13. Magnon C, et al. Autonomic nerve development contributes to prostate cancer progression. Science. 2013; 341:1236361. doi:10.1126/science.1236361. [PubMed: 23846904]
14. Ding Z, et al. SMAD4-dependent barrier constrains prostate cancer growth and metastatic progression. Nature. 2011; 470:269–273. doi:nature09677 [pii]10.1038/nature09677. [PubMed: 21289624]
15. Nandana S, Chung LW. Prostate cancer progression and metastasis: potential regulatory pathways for therapeutic targeting. American journal of clinical and experimental urology. 2014; 2:92–101. [PubMed: 25374910]
16. Cho H, et al. RapidCaP, a novel GEM model for metastatic prostate cancer analysis and therapy, reveals myc as a driver of Pten-mutant metastasis. Cancer Discov. 2014; 4:318–333. doi:10.1158/2159-8290.CD-13-0346. [PubMed: 24444712]
17. Mouchiroud L, Eichner LJ, Shaw RJ, Auwerx J. Transcriptional coregulators: fine-tuning metabolism. Cell Metab. 2014; 20:26–40. doi:10.1016/j.cmet.2014.03.027. [PubMed: 24794975]
18. Lapointe J, et al. Gene expression profiling identifies clinically relevant subtypes of prostate cancer. Proc Natl Acad Sci U S A. 2004; 101:811–816. doi:10.1073/pnas.0304146101. [PubMed: 14711987]
19. Cerami E, et al. The cBio cancer genomics portal: an open platform for exploring multidimensional cancer genomics data. Cancer Discov. 2012; 2:401–404. doi:10.1158/2159-8290.CD-12-0095. [PubMed: 22588877]

20. Gao J, et al. Integrative analysis of complex cancer genomics and clinical profiles using the cBioPortal. Sci Signal. 2013; 6:pl1. doi:10.1126/scisignal.2004088. [PubMed: 23550210]
21. Grasso CS, et al. The mutational landscape of lethal castration-resistant prostate cancer. Nature. 2012; 487:239–243. doi:10.1038/nature11125. [PubMed: 22722839]
22. Taylor BS, et al. Integrative genomic profiling of human prostate cancer. Cancer Cell. 2010; 18:11–22. doi:10.1016/j.ccr.2010.05.026. [PubMed: 20579941]
23. Tomlins SA, et al. Integrative molecular concept modeling of prostate cancer progression. Nat Genet. 2007; 39:41–51. doi:10.1038/ng1935. [PubMed: 17173048]
24. Varambally S, et al. Integrative genomic and proteomic analysis of prostate cancer reveals signatures of metastatic progression. Cancer Cell. 2005; 8:393–406. doi:10.1016/j.ccr.2005.10.001. [PubMed: 16286247]
25. Robinson D, et al. Integrative clinical genomics of advanced prostate cancer. Cell. 2015; 161:1215–1228. doi:10.1016/j.cell.2015.05.001. [PubMed: 26000489]
26. Lin J, Handschin C, Spiegelman BM. Metabolic control through the PGC-1 family of transcription coactivators. Cell Metab. 2005; 1:361–370. doi:10.1016/j.cmet.2005.05.004. [PubMed: 16054085]
27. Haq R, et al. Oncogenic BRAF regulates oxidative metabolism via PGC1alpha and MITF. Cancer Cell. 2013; 23:302–315. doi:10.1016/j.ccr.2013.02.003. [PubMed: 23477830]
28. Vazquez F, et al. PGC1alpha expression defines a subset of human melanoma tumors with increased mitochondrial capacity and resistance to oxidative stress. Cancer Cell. 2013; 23:287–301. doi:10.1016/j.ccr.2012.11.020. [PubMed: 23416000]
29. LeBleu VS, et al. PGC-1alpha mediates mitochondrial biogenesis and oxidative phosphorylation in cancer cells to promote metastasis. Nat Cell Biol. 2014; 16:992–1003. 1001–1015. doi:10.1038/ncb3039. [PubMed: 25241037]
30. LaGory EL, et al. Suppression of PGC-1alpha Is Critical for Reprogramming Oxidative Metabolism in Renal Cell Carcinoma. Cell reports. 2015; 12:116–127. doi:10.1016/j.celrep.2015.06.006. [PubMed: 26119730]
31. D'Errico I, et al. Peroxisome proliferator-activated receptor-gamma coactivator 1-alpha (PGC1alpha) is a metabolic regulator of intestinal epithelial cell fate. Proc Natl Acad Sci U S A. 2011; 108:6603–6608. doi:10.1073/pnas.1016354108. [PubMed: 21467224]
32. Sancho P, et al. MYC/PGC-1alpha Balance Determines the Metabolic Phenotype and Plasticity of Pancreatic Cancer Stem Cells. Cell Metab. 2015; 22:590–605. doi:10.1016/j.cmet.2015.08.015. [PubMed: 26365176]
33. Audet-Walsh E, et al. The PGC-1alpha/ERRalpha Axis Represses One-Carbon Metabolism and Promotes Sensitivity to Anti-folate Therapy in Breast Cancer. Cell reports. 2016; 14:920–931. doi:10.1016/j.celrep.2015.12.086. [PubMed: 26804918]
34. Lin J, et al. Defects in adaptive energy metabolism with CNS-linked hyperactivity in PGC- 1alpha null mice. Cell. 2004; 119:121–135. doi:10.1016/j.cell.2004.09.013S0092867404008864 [pii]. [PubMed: 15454086]
35. Eisele PS, Handschin C. Functional crosstalk of PGC-1 coactivators and inflammation in skeletal muscle pathophysiology. Semin Immunopathol. 2014; 36:27–53. doi:10.1007/s00281-013-0406-4. [PubMed: 24258516]
36. Saint-Geniez M, et al. PGC-1alpha regulates normal and pathological angiogenesis in the retina. Am J Pathol. 2013; 182:255–265. doi:10.1016/j.ajpath.2012.09.003. [PubMed: 23141926]
37. Nardella C, Carracedo A, Salmena L, Pandolfi PP. Faithfull modeling of PTEN loss driven diseases in the mouse. Curr Top Microbiol Immunol. 2011; 347:135–168. doi:10.1007/82_2010_62. [PubMed: 20549475]
38. Nardella C, et al. Aberrant Rheb-mediated mTORC1 activation and Pten haploinsufficiency are cooperative oncogenic events. Genes Dev. 2008; 22:2172–2177. doi:22/16/2172 [pii]10.1101/gad.1699608. [PubMed: 18708577]
39. Li S, et al. Genome-wide coactivation analysis of PGC-1alpha identifies BAF60a as a regulator of hepatic lipid metabolism. Cell Metab. 2008; 8:105–117. doi:10.1016/j.cmet.2008.06.013. [PubMed: 18680712]

40. Tennakoon JB, et al. Androgens regulate prostate cancer cell growth via an AMPK-PGC- 1alpha-mediated metabolic switch. Oncogene. 2014; 33:5251–5261. doi:10.1038/onc.2013.463. [PubMed: 24186207]
41. Shiota M, et al. Peroxisome proliferator-activated receptor gamma coactivator-1alpha interacts with the androgen receptor (AR) and promotes prostate cancer cell growth by activating the AR. Mol Endocrinol. 2010; 24:114–127. doi:10.1210/me.2009-0302. [PubMed: 19884383]
42. Buijs JT, van der Pluijm G. Osteotropic cancers: from primary tumor to bone. Cancer Lett. 2009; 273:177–193. doi:10.1016/j.canlet.2008.05.044. [PubMed: 18632203]
43. Garcia M, et al. Cyclooxygenase-2 inhibitor suppresses tumour progression of prostate cancer bone metastases in nude mice. BJU Int. 2014; 113:E164–177. doi:10.1111/bju.12503. [PubMed: 24127882]
44. Feige JN, Auwerx J. Transcriptional coregulators in the control of energy homeostasis. Trends Cell Biol. 2007; 17:292–301. doi:10.1016/j.tcb.2007.04.001. [PubMed: 17475497]
45. Finley LW, Zhang J, Ye J, Ward PS, Thompson CB. SnapShot: cancer metabolism pathways. Cell Metab. 2013; 17:466–466. e462. doi:10.1016/j.cmet.2013.02.016. [PubMed: 23473039]
46. Stein RA, et al. Estrogen-related receptor alpha is critical for the growth of estrogen receptor-negative breast cancer. Cancer Res. 2008; 68:8805–8812. doi:10.1158/0008-5472.CAN-08-1594. [PubMed: 18974123]
47. Gaillard S, et al. Receptor-selective coactivators as tools to define the biology of specific receptor-coactivator pairs. Mol Cell. 2006; 24:797–803. doi:10.1016/j.molcel.2006.10.012. [PubMed: 17157261]
48. Chang CY, et al. The metabolic regulator ERRalpha, a downstream target of HER2/IGF-1R, as a therapeutic target in breast cancer. Cancer Cell. 2011; 20:500–510. doi:10.1016/j.ccr.2011.08.023. [PubMed: 22014575]
49. Piskounova E, et al. Oxidative stress inhibits distant metastasis by human melanoma cells. Nature. 2015; 527:186–191. doi:10.1038/nature15726. [PubMed: 26466563]
50. Lunt SY, Vander Heiden MG. Aerobic glycolysis: meeting the metabolic requirements of cell proliferation. Annu Rev Cell Dev Biol. 2011; 27:441–464. doi:10.1146/annurev-cellbio-092910-154237. [PubMed: 21985671]
51. Carracedo A, et al. A metabolic prosurvival role for PML in breast cancer. The Journal of clinical investigation. 2012; 122:3088–3100. doi:62129 [pii]10.1172/JCI62129. [PubMed: 22886304]
52. Schafer ZT, et al. Antioxidant and oncogene rescue of metabolic defects caused by loss of matrix attachment. Nature. 2009; 461:109–113. doi:nature08268 [pii]10.1038/nature08268. [PubMed: 19693011]
53. Arroyo-Berdugo Y, et al. Involvement of ANXA5 and ILKAP in susceptibility to malignant melanoma. PLoS One. 2014; 9:e95522. doi:10.1371/journal.pone.0095522. [PubMed: 24743186]
54. Song MS, et al. Nuclear PTEN regulates the APC-CDH1 tumor-suppressive complex in a phosphatase-independent manner. Cell. 2011; 144:187–199. doi:S0092-8674(10)01473-X [pii]10.1016/j.cell.2010.12.020. [PubMed: 21241890]
55. Chen Z, et al. Differential p53-independent outcomes of p19(Arf) loss in oncogenesis. Sci Signal. 2009; 2:ra44. doi:2/84/ra44 [pii]10.1126/scisignal.2000053. [PubMed: 19690330]
56. Nardella C, et al. Differential requirement of mTOR in postmitotic tissues and tumorigenesis. Sci Signal. 2009; 2:ra2. doi:2/55/ra2 [pii]10.1126/scisignal.2000189. [PubMed: 19176516]
57. Guiu M, Arenas EJ, Gawrzak S, Pavlovic M, Gomis RR. Mammary cancer stem cells reinitiation assessment at the metastatic niche: the lung and bone. Methods Mol Biol. 2015; 1293:221–229. doi:10.1007/978-1-4939-2519-3_13. [PubMed: 26040691]
58. Carracedo A, et al. Inhibition of mTORC1 leads to MAPK pathway activation through a PI3K-dependent feedback loop in human cancer. J Clin Invest. 2008; 118:3065–3074. doi:10.1172/JCI34739. [PubMed: 18725988]
59. Ugalde-Olano A, et al. Methodological aspects of the molecular and histological study of prostate cancer: focus on PTEN. Methods. 2015; 77-78:25–30. doi:10.1016/j.ymeth.2015.02.005. [PubMed: 25697760]

60. Finley LW, et al. SIRT3 Opposes Reprogramming of Cancer Cell Metabolism through HIF1alpha Destabilization. Cancer Cell. 2011; 19:416–428. doi:S1535-6108(11)00085-7 [pii]10.1016/j.ccr.2011.02.014. [PubMed: 21397863]

61. Caro-Maldonado A, et al. Metabolic reprogramming is required for antibody production that is suppressed in anergic but exaggerated in chronically BAFF-exposed B cells. J Immunol. 2014; 192:3626–3636. doi:10.4049/jimmunol.1302062. [PubMed: 24616478]

62. Wojtala A, et al. Methods to monitor ROS production by fluorescence microscopy and fluorometry. Methods Enzymol. 2014; 542:243–262. doi:10.1016/B978-0-12-416618-9.00013-3. [PubMed: 24862270]

63. Ittmann M, et al. Animal models of human prostate cancer: the consensus report of the New York meeting of the Mouse Models of Human Cancers Consortium Prostate Pathology Committee. Cancer Res. 2013; 73:2718–2736. doi:10.1158/0008-5472.CAN-12-4213. [PubMed: 23610450]

64. Liu X, et al. High resolution metabolomics with acyl-CoA profiling reveals widespread remodeling in response to diet. Mol Cell Proteomics. 2015 doi:10.1074/mcp.M114.044859.

65. Liu X, Ser Z, Locasale JW. Development and quantitative evaluation of a high-resolution metabolomics technology. Analytical chemistry. 2014; 86:2175–2184. doi:10.1021/ac403845u. [PubMed: 24410464]

66. Shestov AA, et al. Quantitative determinants of aerobic glycolysis identify flux through the enzyme GAPDH as a limiting step. eLife. 2014; 3 doi:10.7554/eLife.03342.

67. Rodriguez RM, et al. Regulation of the transcriptional program by DNA methylation during human alphabeta T-cell development. Nucleic Acids Res. 2015; 43:760–774. doi:10.1093/nar/gku1340. [PubMed: 25539926]

68. Bergmann R, Ludbrook J, Spooren WPJM. Statistical Computing and Graphics: Different Outcomes of the Wilcoxon—Mann—Whitney Test from Different Statistics Packages. The American Statistician. 2000; 54:72–77. doi:10.1080/00031305.2000.10474513.

69. Quinn, G.; Keough, M. Experimental design and data analysis for biologists. Cambridge University Press; 2002.

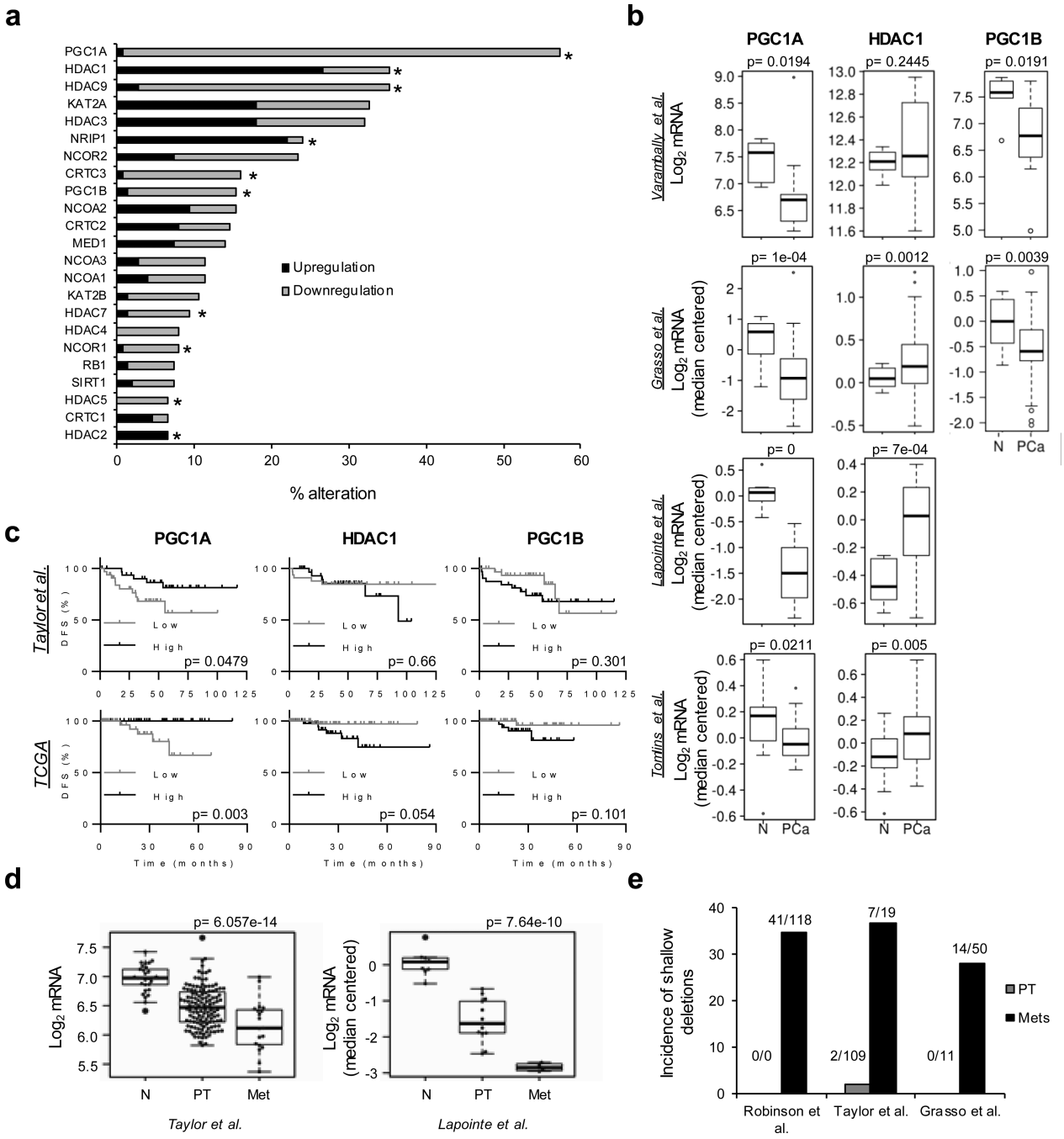

Figure 1. PGC1A is down-regulated in prostate cancer

a, Frequency of alterations (differences greater than 2-fold *vs.* mean expression of non-tumoural biopsies) in the expression of 23 master co-regulators of metabolism in a cohort of 150 PCa patients[22]. *, statistically different expression ($p<0.05$) of the indicated gene in PCa (n=150) *vs.* normal (n=29) patient specimens (according to Supplementary Fig. 1A). **b**, Gene expression levels of *PGC1A*, *PGC1B* and *HDAC1* in up to four additional PCa datasets (N: normal; PCa: prostate cancer). Sample size: Tomlins (Normal=23; PCa=52); Grasso (Normal=12; PCa=76); Lapointe (Normal=9; PCa=17); Varambally (Normal=6;

PCa=13). **c**, Association of the indicated genes with disease-free survival (DFS) in two PCa datasets (Low: 1st quartile distribution; High: 4th quartile distribution) (Sample size: TCGA provisional data[19,20], primary tumours n=240; Taylor[22], primary tumours n=131). **d**, *PGC1A* expression in normal prostate (N), primary tumour (PT) and metastatic (Met) specimens in Taylor and Lapointe datasets[18,22]. Sample size: Taylor N=29, PT=131 and Met=19; Lapointe N=9, PT=13 and Met=4. **e**, Incidence of *PGC1A* shallow deletions in three independent datasets[21,22,25]. Points outlined by circles indicate statistical outliers (d). Error bars represent minimum and maximum values (b and d). p, p-value. Statistic test: two-tailed Student T test (a, b), Kaplan-Meier estimator (c, DFS) and ANOVA (d).

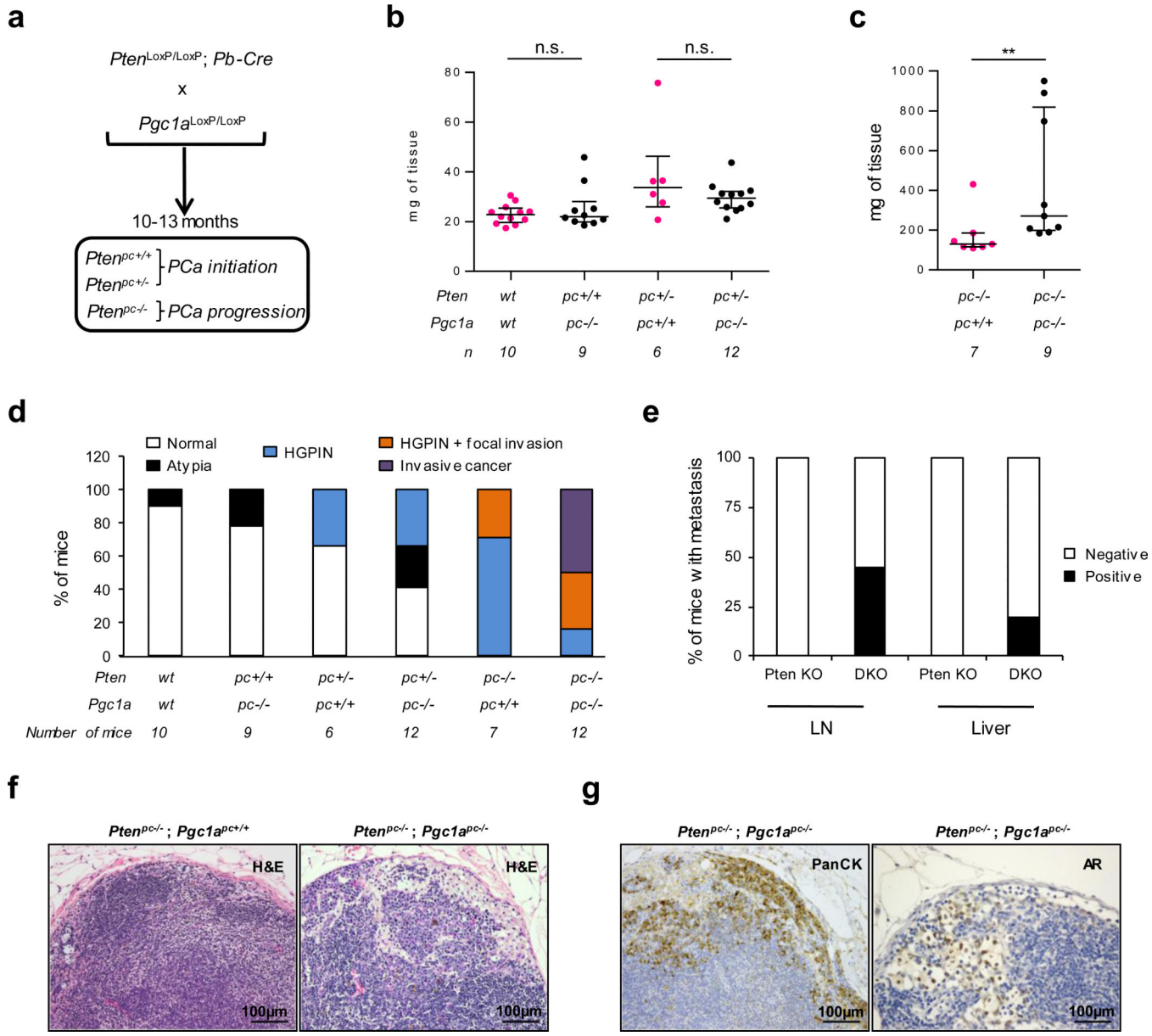

Figure 2. Combined deletion of *Pgc1a* and *Pten* in the murine prostate epithelia results in prostate cancer progression and dissemination

a, Schematic representation of the genetic cross and the time of analysis. **b-c**, Comparison of anterior prostate lobe weights (when both anterior lobes were analysed, the average was calculated and represented) between genotypes (*Pten*^{wt} *Pgc1a*^{wt} n=10 mice; *Pten*$^{pc+/+}$ *Pgc1a*$^{pc-/-}$ n=9 mice; *Pten*$^{pc+/-}$ *Pgc1a*$^{pc+/+}$ n=6 mice; *Pten*$^{pc+/-}$ *Pgc1a*$^{pc-/-}$ n=12 mice; *Pten* $^{pc-/-}$ *Pgc1a*$^{pc+/+}$ n=7 mice; *Pten*$^{pc-/-}$ *Pgc1a*$^{pc-/-}$ n=9 mice; pc, prostate-specific allelic changes; +, Wildtype allele; −, deleted allele; wt: any given genotype resulting in the lack of deletion of *Pgc1a* or *Pten* alleles). **d**, Histopathological characterization of the prostate (HGPIN: High-grade prostatic intraepithelial neoplasia) in the indicated genotypes (*Pten*^{wt} *Pgc1a*^{wt} n=10 mice; *Pten*$^{pc+/+}$ *Pgc1a*$^{pc-/-}$ n=9 mice; *Pten*$^{pc+/-}$ *Pgc1a*$^{pc+/+}$ n=6 mice; *Pten*$^{pc+/-}$ *Pgc1a*$^{pc-/-}$ n=12 mice; *Pten* $^{pc-/-}$ *Pgc1a*$^{pc+/+}$ n=7 mice; *Pten*$^{pc-/-}$ *Pgc1a*$^{pc-/-}$ n=12

mice; pc, prostate-specific allelic changes; +, Wildtype allele; −, deleted allele; wt: any given genotype resulting in the lack of deletion of *Pgc1a* or *Pten* alleles). **e**, Quantification of the frequency of metastatic lesions in lymph nodes (LN) and liver of *Pten* KO (5 mice) and DKO (9 mice) mice. **f**, Representative histological images (200X) of LN with (right panel) and without (left panel) metastasis in the indicated genotypes. **g**, Representative immunohistochemical detection (200X) of Pan-cytokeratin (PanCK) and androgen receptor (AR) positive cells in metastatic LN of DKO mice. DKO; $Pten^{pc-/-}$, $Pgc1a^{pc-/-}$. n.s.: not significant; **p<0.01. H&E: Haematoxylin-eosin. Error bars indicate median with interquartile range (b, c). Statistic test: two-tailed Mann Whitney U test (b, c).

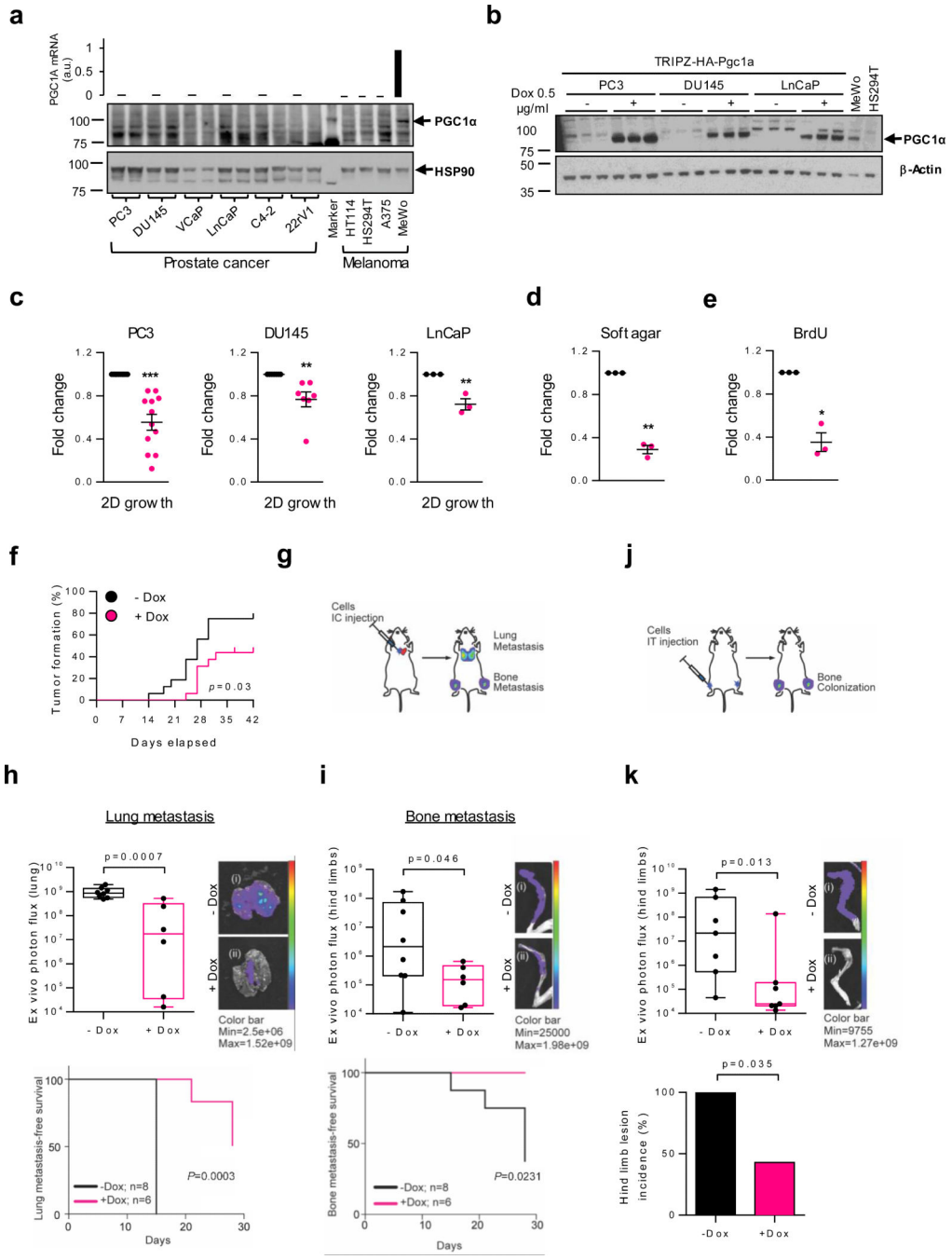

Figure 3. PGC1α exhibits tumour and metastasis suppressive activity in PCa cell lines

a, Analysis of PGC1α expression by qRT-PCR (top histogram) and western blot in a panel of prostate cancer cell lines (technical duplicates are shown), using melanoma cell lines as positive (MeWo) and negative (HT114, HS294T and A375) controls (n=3, independent experiments). **b**, Representative experiment of PGC1α expression in PC3, DU145 and LnCaP cell lines after treatment with 0.5 µg/ml doxycycline (Dox) (similar results were obtained in three independent experiments). **c**, Relative cell number quantification in Pgc1α expressing and non-expressing cells. Data is represented as cell number at day 6 relative to −

Dox cells (n=12 in PC3; n=7 in DU145; n=3 in LnCaP, independent experiments). **d-e**, Effect of Pgc1α expression on anchorage-independent growth (d; n=3, independent experiments) and BrdU incorporation (e; n=3, independent experiments) in PC3 cells. **f**, Evaluation of tumour formation in xenotransplantation experiments (n=7 mice; 2 injections per mouse). **g**, Schematic representation of metastasis assay through intra-cardiac injection. **h-i**, Evaluation of metastatic capacity of Pgc1α-expressing PC3 cells using intra-cardiac xenotransplant assays (n=8 mice for − Dox and n=6 mice for + Dox). Luciferase-dependent signal intensity (upper panels) and metastasis-free survival curves (lower panels) of PCa cells in lungs (h) and limbs (i) was monitored for up to 28 days. Representative luciferase images are presented referred to the quantification plots. In hind limb photon flux analysis, average signal from two limbs per mouse is presented. (i) and (ii) depict tibia photon flux images from specimens that are proximal to the median signal in − Dox and + Dox, respectively. **j**, Schematic representation of bone metastasis assay through intra-tibial injection. **k**, Evaluation of the metastatic capacity of Pgc1α-expressing PC3 cells using intra-tibial xenotransplant assays (n=7 mice) Photon flux quantification at 20 days (upper panel) and incidence of metastatic lesions at the end point (lower panel). Representative luciferase images are presented referred to the quantification plots. For photon flux analysis, average signal from two limbs per mouse is presented. For incidence analysis, mice with at least one limb yielding luciferase signal > 50.000 units were considered metastasis-positive. (i) and (ii) depict tibia photon flux images from specimens that are proximal to the median signal in − Dox and + Dox, respectively. + Dox: Pgc1α induced conditions; − Dox: Pgc1α non-expressing conditions. Error bars represent standard deviation of the mean (c), s.e.m. (d, e) or median with interquartile range (h-k). Statistic tests: two-tailed Student T test (c, d and e), one-tailed Mann-Whitney U test h, i and k (upper panels)), log-rank test (f, h and i (lower panels)) and Fisher's exact test (k, lower panels). *p*, p-value. *p < 0.05, **p < 0.01, ***p < 0.001. Statistics source data for Fig. 3k are provided in Supplementary Table 9.

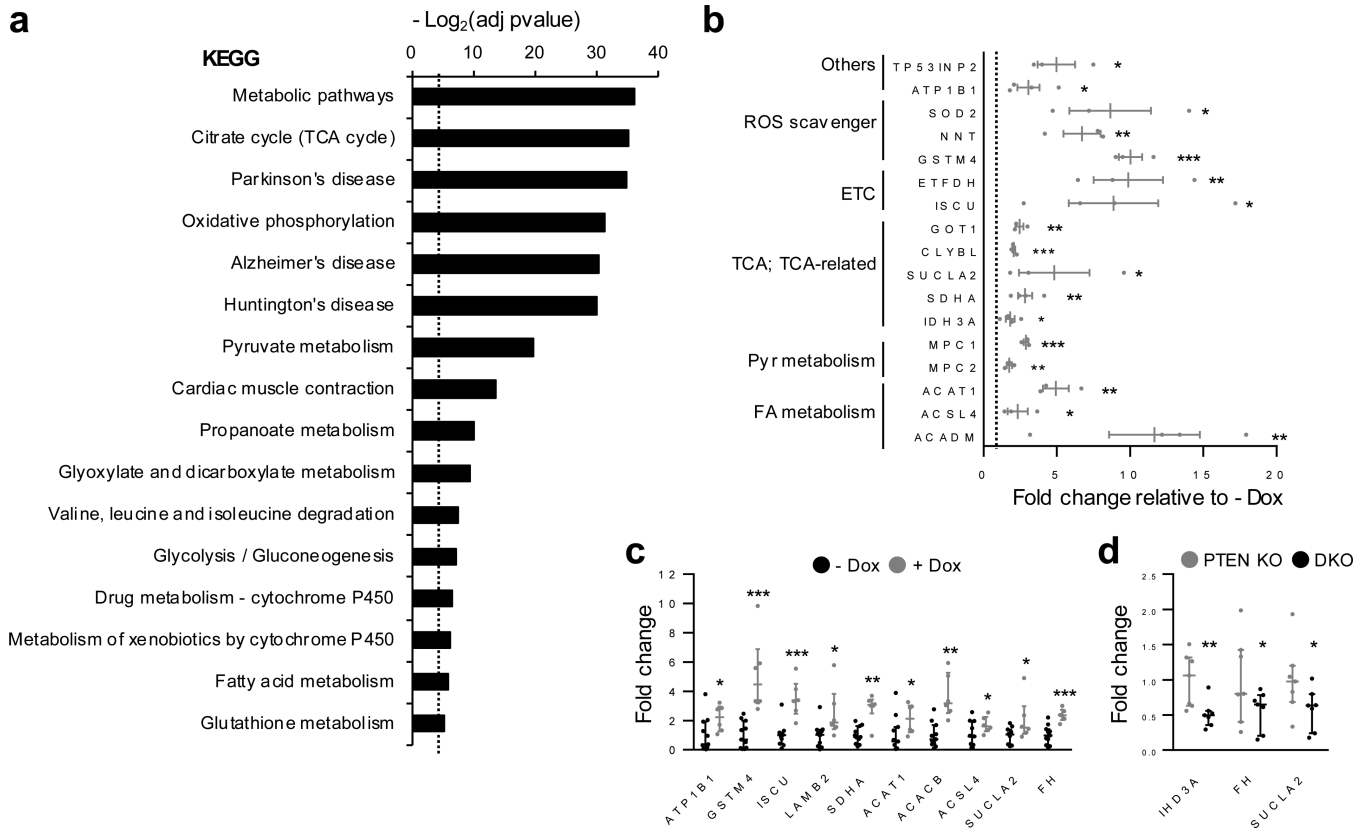

Figure 4. PGC1α induces a metabolic transcriptional program

a, KEGG (Kyoto Encyclopaedia of Genes and Genomes) analysis of the transcriptional program regulated by PGC1α. Red dotted line indicates p=0.05. **b-d**, Validation of microarray by qRTPCR in PC3 TRIPZ-HA-Pgc1a cells (**b**, n=3 for TP53INP2, SOD2, NNT, GSTM4, ETFDH, GOT1, CLYBL, SUCLA2, MPC1, MPC2, ACAT1 and ACSL4; n=4 for ATP1B1, ISCU, SDHA, IDH3A and ACADM; independent experiments; data is normalised to − Dox condition, represented by a black dotted line), xenograft samples (**c**, − Dox n=11 tumours; + Dox n=6 tumours) and prostate tissue samples from *Pten* KO and DKO mice (**d**, n=7 mice). Adj pvalue: adjusted p-value; +Dox: Pgc1α induced conditions; −Dox: Pgc1α non-expressing conditions; *Pten* KO: $Pten^{pc-/-}$, $Pgc1a^{pc+/+}$; DKO: $Pten^{pc-/-}$, $Pgc1a^{pc-/-}$. Error bars indicate s.e.m. (b) or median with interquartile range (c, d). Statistic tests: one-tail Student T test (b); one-tail Mann Whitney U test (c, d). *p < 0.05, **p < 0.01, ***p < 0.001.

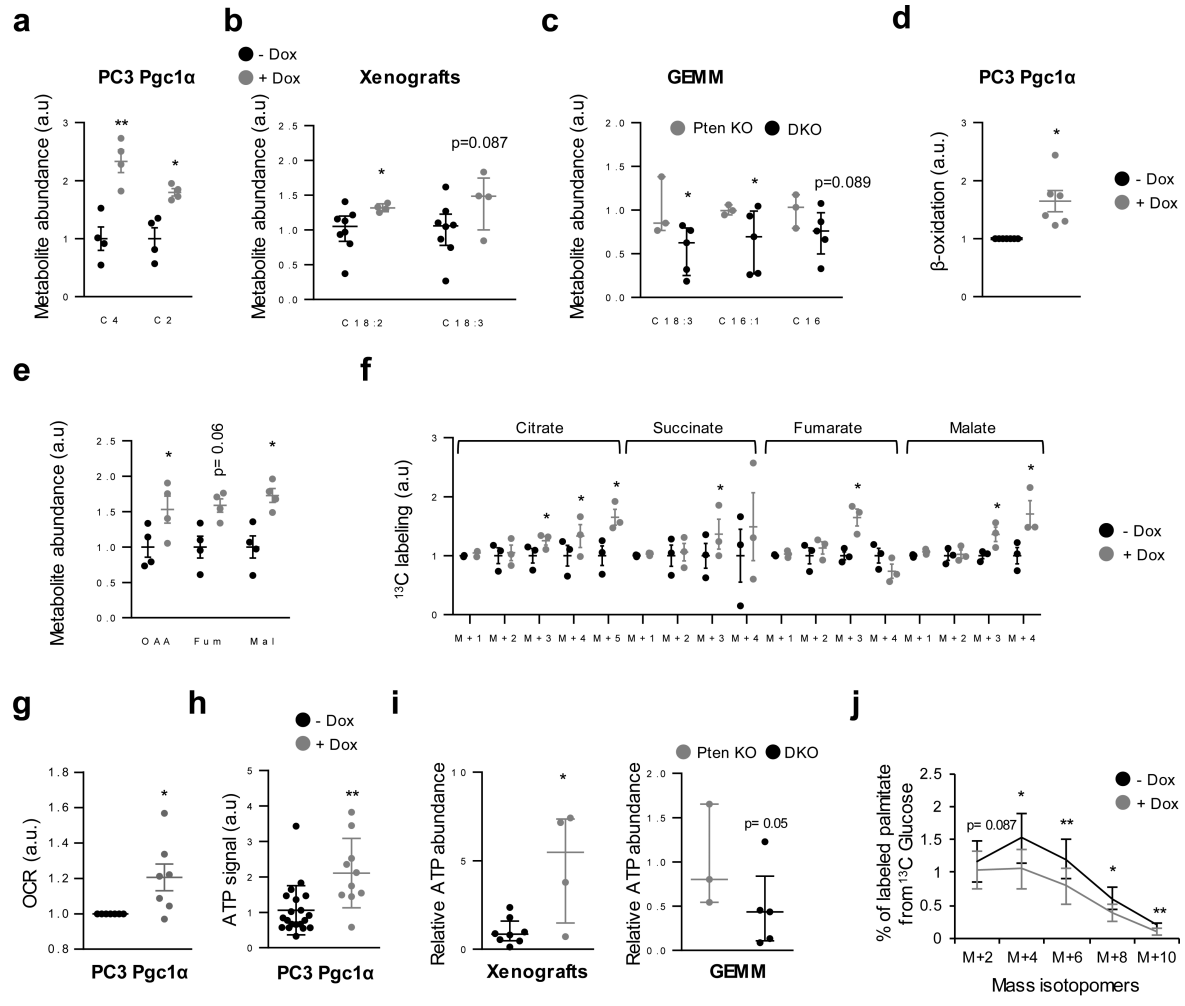

Figure 5. PGC1α induces a catabolic metabolic program

a-c, Untargeted LC-HRMS analysis of differential abundance in metabolites involved in fatty acid catabolism in Pgc1α-expressing PC3 cells (a, n=4, independent experiments), xenograft (b, − Dox n=8 tumours; + Dox n=4 tumours) and GEMM (c, *Pten* KO n=3 mice; DKO n=5 mice). **d**, Evaluation of the dehydrogenation of tritiated palmitate (readout of β-oxidation) in PC3 cells upon Pgc1α expression (n=6, independent experiments). **e**, Effect of Pgc1α expression on the abundance TCA intermediates measured by LC-HRMS in PC3 cells (n=4, independent experiments). **f**, Effect of Pgc1α expression on tricarboxylic acid

cycle (TCA) intermediates (mass isotopomer abundance) after stable ^{13}C-U_6-Glucose labelling in PC3 cells (n=3, independent experiments). **g**, Oxygen consumption rate (OCR) in PC3 Pgc1α expressing cells (n=7, independent experiments). **h**, Basal mitochondrial ATP production in PC3 cells upon Pgc1α expression (n=20 for − Dox and n=10 for + Dox conditions, independent experiments). **i**, LC-HRMS quantification of ATP abundance in xenografts (left panel, − Dox n=8 tumours; + Dox n=4 tumours) and GEMM (right panel, *Pten* KO n=3 mice; DKO n=5 mice). **j**, Effect of Pgc1α expression on palmitate paired mass isotopomer abundance after stable ^{13}C-U_6-Glucose labelling in PC3 cells (n=3, independent experiments). **k,** Schematic representation of the main findings of the study. Pyr: pyruvate; AcCoA; acetyl CoA; OAA: oxaloacetate; Mal: malate; Fum: fumarate; Succ: succinate; Cit: citrate; ETC: electron transport chain; TCA: tricarboxylic acid cycle; FA: fatty acids. a.u.: arbitrary units; Mal: malate; Fum: fumarate; OAA: oxaloacetate. Error bars indicate s.e.m. (a, d, e, f, h, j), standard deviation of the mean (g) or median with interquartile range (b, c, i). Statistic tests: two-tail Student T test (a, d, e, f, g, h, j); one-tail Mann Whitney U test (b, c, i). *$p < 0.05$, **$p < 0.01$, ***$p < 0.001$.

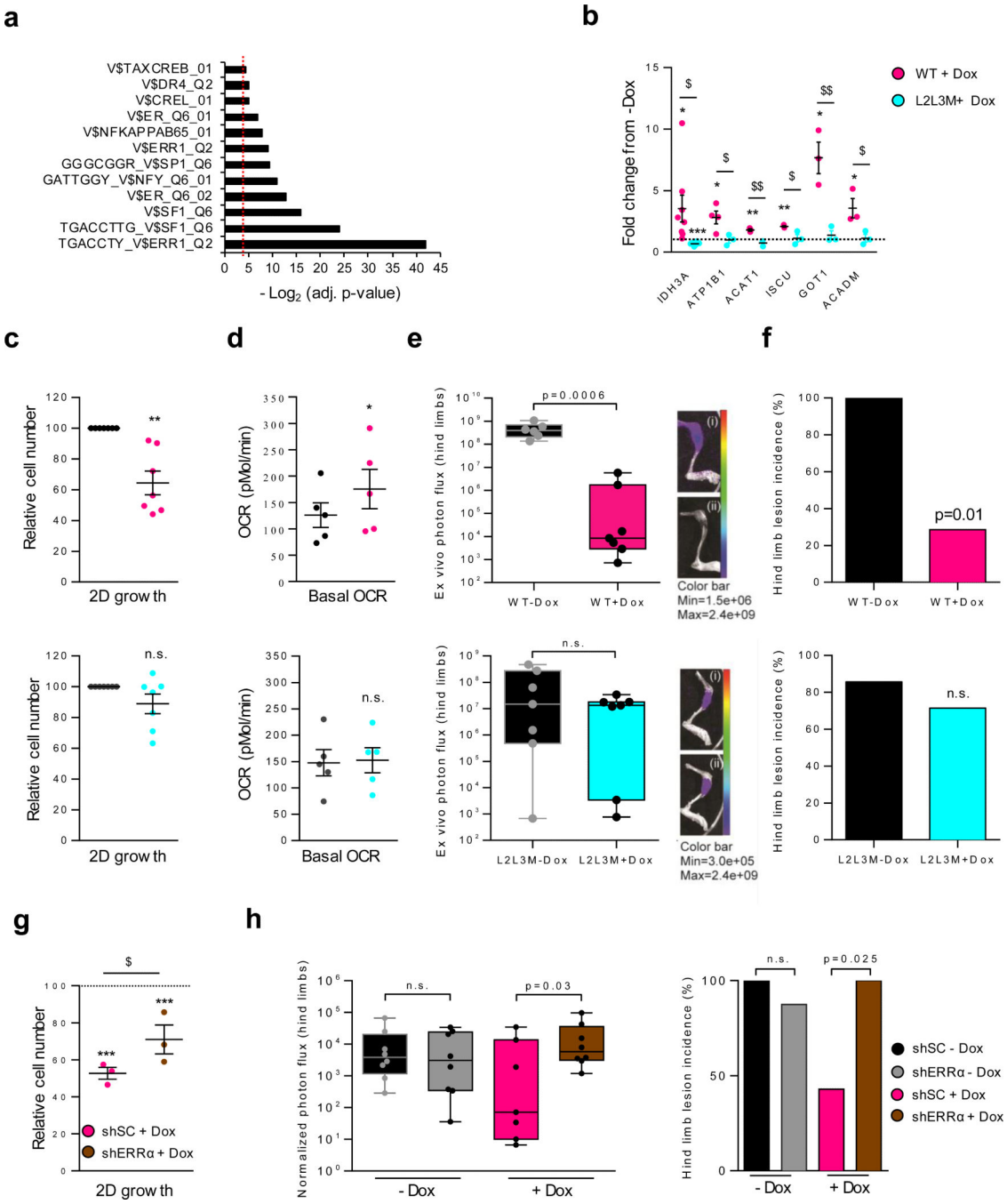

Figure 6. An ERRα-dependent transcriptional program mediates the tumour suppressive activity of PGC1α

a, Promoter enrichment analysis of the PGC1α transcriptional program. Red dotted line indicates p=0.05. **b-d**, Effect of $Pgc1\alpha^{WT}$ or $Pgc1\alpha^{L2L3M}$ induction on the expression of indicated genes (b, qRTPCR; n=8 for IDH3A; n=4 for ATP1B1; n=3 for ACAT1, ISCU, GOT1 and ACADM genes, independent experiments; data is normalised to each − Dox condition, represented by a black dotted line), relative cell number by crystal violet (c, n=7, independent experiments) and oxygen consumption rate (d, OCR, n=5, independent

experiments). **e-f**, Evaluation of the metastatic capacity of PC3 Pgc1α^{WT} (upper panels) or PC3 Pgc1α^{L2L3M} (lower panels) expressing cells using intra-tibial xenotransplant assays (e, photon flux quantification, WT, n=6 mice and L2L3M, n=7 mice, 2 hind limb per mice; f, incidence of metastatic lesions presented as histograms). Representative luciferase images are presented referred to the quantification plots. For photon flux analysis, average signal from two limbs per mouse is presented. For incidence analysis, mice with at least one limb yielding luciferase signal > 50.000 units were considered metastasis-positive. (i) and (ii) depict tibia photon flux images from specimens that are proximal to the median signal in − Dox and + Dox, respectively. **g**, Relative cell number quantification upon ERRα silencing in PC3 Pgc1α expressing cells. Data is represented as cell number at day 4 relative to − Dox cells (n=3, independent experiments). **h,** Evaluation of metastatic capacity of Pgc1α-expressing PC3 cells transduced with shSC or shERRα using intra-tibial implantation for 14 days (n=8 mice; 2 injections per mice; incidence of metastatic lesions presented as histograms). Representative luciferase images are presented referred to the quantification plots. For photon flux analysis (left panel), average signal from two limbs per mouse is presented. For incidence analysis (right panel), mice with at least one limb yielding luciferase signal > 50.000 units were considered metastasis-positive. Adj. p-value: adjusted p-value. +Dox: Pgc1α induced conditions; −Dox: Pgc1α non-expressing conditions. Min: minimum. Max: maximum. n.s.: not significant. Error bars represent s.e.m. (b, c, d, g) or median with interquartile range (e, h). Statistic tests: one-tailed Student T test (b, c, d, g); one-tailed Mann-Whitney U test (e, h (left panel)); Fisher exact test (f, h (right panel)). */$ $p < 0.05$, **/$$ $p < 0.01$, ***/$$$ $p < 0.001$. Asterisks indicate statistical difference between – Dox and + Dox conditions and dollar symbol between Pgc1α^{WT} and Pgc1α^{L2L3M} or shSC and shERRα. Statistics source data for Fig. 6e,h are provided in Supplementary Table 9.

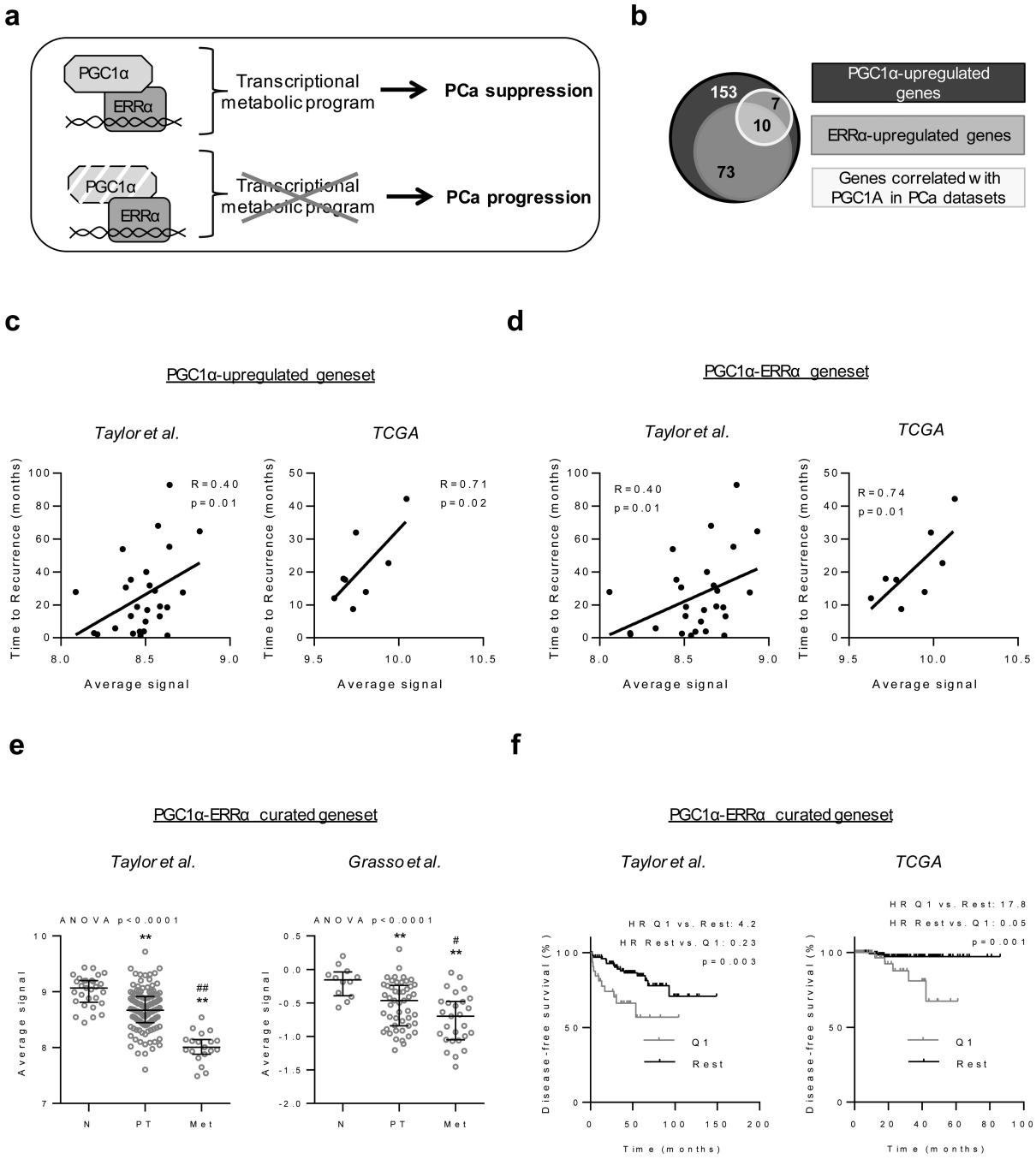

Figure 7. The PGC1α transcriptional program is associated with prostate cancer recurrence

a, Schematic summary of the ERRα-dependent regulation of PGC1α transcriptional metabolic program, and its association with PCa progression. Dashed PGC1α box (pink) represents a decrease in abundance. **b**, Venn diagram showing the distribution of PGC1α target genes, ERRα target genes and genes correlated with *PGC1A* expression in PCa patient specimens (from Supplementary Table 7). **c-d**, Correlation between time to recurrence and the average signal of the genes within the PGC1α-upregulated gene set (c) or the PGC1α-dependent ERRα-upregulated gene set (d) in the indicated datasets[19,20,22]

(Taylor n=27; TCGA provisional dataset n=8). Each dot corresponds to an individual patient specimen. **e**, Representation of the average signal of the genes within the "PGC1α-ERRα curated gene set" (Supplementary Table 7) in normal (N; Taylor n=29 and Grasso n=12), primary tumours (PT; Taylor n=131 and Grasso n=49) and metastasis (Met; Taylor n=19 and Grasso n=27), in two independent datasets[21,22]. Each dot corresponds to an individual patient specimen. **f**, Association of the "PGC1α-ERRα signature" with disease-free survival (DFS) in the indicated patient datasets[19,20,22] (Taylor n=131; TCGA provisional dataset n=240). Q1 indicates patients with signature signal within the first quartile of primary tumours in the corresponding dataset. Error bars indicate s.e.m. Statistic test: Pearson's coefficient (*R*) (c and d), ANOVA (e) and Kaplan-Meier estimator (f).